Journal of Physics G: Nuclear and Particle Physics

物理学杂志 G:核物理学和粒子物理学

J.Phys. G: Nucl.Part.Phys. 47 (2020) 045108 (35pp) https://doi.org/10.1088/1361-6471/ab4dbe

J.物理 G: Nucl。部分。https://doi.org/10.1088/1361-6471/ab4dbe 物理 47 (2020) 045108 (35pp)

Topological background discrimination in the PandaX-III neutrinoless double beta decay experiment

拓扑背景鉴别潘达三号无中微子双β衰变实验

J Galan, X Chen, H Du, C Fu, K Giboni, F Giuliani, K Han, B Jiang, X Ji, H Lin, Y Lin, J Liu,

加兰，陈，杜，基波尼，朱利安尼，韩，江，季，林，刘，

K Ni, X Ren, S Wang, S Wu, C Xie, Y Yang, T Zhang,

倪，任，王，吴，谢，杨，张，

L Zhao, S Aune, Y Bedfer, E Berthoumieux, D Calvet, N d'Hose, E Ferrer-Ribas, F Kunne, B Manier, D Neyret,

赵，S Aune，Y Bedfer，E Berthoumieux，D，N d'Hose，E Ferrer-Ribas，F Kunne，B Manier，D Neyret，

T Papaevangelou, L Chen, S Hu, P Li, X Li, H Zhang,

陈，胡，李，李，张，

M Zhao, J Zhou, Y Mao, H Qiao, S Wang, Y Yuan,

男，赵，周俊杰，毛友友，乔海平，王树声，袁友友，

M Wang, Y Chen, A N Khan, J Tang, W Wang,

王，陈，单于，唐，王，

H Chen, C Feng, J Liu, S Liu, X Wang, D Zhu,

陈海峰，刘俊杰，刘 s，王，朱，

J F Castel, S Cebrián, T Dafni, I G Irastorza, G Luzón, H Mirallas, X Sun, A Tan, W Haxton, Y Mei, C Kobdajand Y Yan

卡斯特尔、塞布里安、达芬尼、伊拉斯托扎、吕宋、米拉拉斯、孙、阿坦、阿克斯顿、梅、科布达雅和严

INPAC and School of Physics and Astronomy, Shanghai Jiao Tong University, Shanghai Laboratory for Particle Physics and Cosmology, Shanghai 200240, People's Republic of China

INPAC 与上海交通大学物理与天文学院，上海粒子物理与宇宙学实验室，上海 200240，中华人民共和国

IRFU, CEA, Université Paris-Saclay, F-91191 Gif-sur-Yvette, France Department of Physics, University of Maryland, College Park, MD 20742, United States of America

IRFU，CEA，巴黎大学萨克莱分校，F-91191 Gif-sur-Yvette，法国物理系，马里兰大学，学院公园，医学博士 20742，美利坚合众国

China Institute of Atomic Energy, Beijing 102413, People's Republic of China School of Physics, Peking University, Beijing 100871, People's Republic of China 6 School of Physics and Key Laboratory of Particle Physics and Particle Irradiation (MOE), Shandong University, Jinan 250100, People's Republic of China School of Physics and Engineering, Sun Yat-Sen University, Guangzhou 510275, People's Republic of China Department of Modern Physics, University of Science and Technology of China, Hefei 230026,People's Republic of China State Key Laboratory of Particle Detection and Electronics, University of Science and Technology of China, Hefei 230026, People's Republic of China University of Zaragoza, C/P Cerbuna 12, E-50009, Zaragoza, Spain 11College of Physical Science and Technology, Central China Normal University, Wuhan 430079, People's Republic of China Nuclear Science Division, Lawrence Berkeley National Laboratory, Berkeley, CA 94720, United States of America

中国原子能科学研究院，北京 102413，中华人民共和国物理学院，北京大学，北京 100871，中华人民共和国第六物理学院及粒子物理与粒子辐照重点实验室，山东大学，济南 250100，中华人民共和国物理与工程学院，中山大学，广州 510275，中华人民共和国现代物理系，中国科学技术大学，合肥 230026，中华人民共和国粒子探测与电子学国家重点实验室，中国科学技术大学，合肥 230026，中华人民共和国萨拉戈萨大学，C/P Cerbuna 12，E-50009，西班牙萨拉戈萨 11 物理科学与技术学院，华中师范大学，武汉 430079，中华人民共和国核科学部，美国加州伯克利劳伦斯伯克利国家实验室，伯克利 94720

Center for Excellence in High Energy Physics and Astrophysics, Suranaree University of Technology, Nakhon Ratchasima 30000, Thailand

泰国纳洪拉特恰希马 30000 苏拉纳雷理工大学高能物理和天体物理学卓越中心

0954-3899/20/045108+35$33.00 2020 IOP Publishing Ltd Printed in the UK 1

0954-3899/20/045108+35 $ 33.00 2020 英国印刷出版有限公司 1

J.Phys. G: Nucl.Part.Phys. 47 (2020) 045108 J Galan et al

J.物理 G: Nucl。部分。《物理》47 (2020) 045108 J Galan 等人

E-mail: javier.galan.lacarra@cern.ch

电子邮件:javier.galan.lacarra@cern.ch

Received 31 July 2019

2019 年 7 月 31 日收到

Accepted for publication 15 October 2019 Published 27 February 2020

2019 年 10 月 15 日接受出版，2020 年 2 月 27 日出版

Abstract

摘要

The PandaX-III experiment plans to search for neutrinoless double beta decay (0νββ) of Xe in the China JinPing underground Laboratory (CJPL).The experiment will use a high pressure gaseous time projection chamber (TPC) to register both the energy and the electron track topology of an event.This article is devoted to demonstrate our particular detector setup capabilities for the identification of 0νββ and the consequent background reduction.As software tool we use REST, a framework developed for the reconstruction and simulation of TPC-based detector systems.We study the potential for background reduction by introducing appropriate parameters based on the properties of 0νββ events.We exploit for the first time not only the energy density of the electron track-ends, but also the electron scattering angles produced by an electron near the end of its trajectory.To implement this, we have added new algorithms for detector signal and track processing inside REST.Their assessment shows that background can be reduced by about 7 orders of magnitude while keeping 0νββ efficiency above 20% for the PandaX-III baseline readout scheme, a two-dimensional 3 mm pitch stripped readout.More generally, we use the potential of REST to handle 2D/3D data to assess the impact on signal-to-background significance at different detector granularities, and to validate the PandaX-III baseline choice.Finally, we demonstrate the additional potential to discriminate surface background events generated at the readout plane in the absence of to, by making use of event parameters related with the diffusion of electrons.

PandaX-III 实验计划在中国金平地下实验室(CJPL)寻找 Xe 的无中微子双 β 衰变(0νββ)。该实验将使用高压气体时间投影室(TPC)记录事件的能量和电子轨道拓扑。本文致力于演示我们特殊的检测器设置能力，用于识别 0νβββ 和随后的背景减少。作为软件工具，我们使用 REST，这是一个为重建和模拟基于 TPC 的探测器系统而开发的框架。我们基于 0νββ 事件的性质，通过引入适当的参数来研究背景减少的可能性。我们第一次不仅利用了电子轨道末端的能量密度，还利用了电子在其轨道末端附近产生的电子散射角。为了实现这一点，我们在 REST 中添加了新的检测器信号和轨道处理算法。他们的评估表明，对于 PandaX-III 基线读出方案，一种二维 3 毫米间距剥离读出，在保持 0νββ 效率高于 20%的同时，背景可以减少约 7 个数量级。更一般地说，我们使用 REST 的潜力来处理 2D/3D 数据，以评估不同探测器粒度对信号-背景显著性的影响，并验证 PandaX-III 基线选择。最后，我们通过利用与电子扩散相关的事件参数，证明了在没有 to 的情况下鉴别在读出平面上产生的表面背景事件的附加潜力。

Keywords: neutrino, PandaX-III, topology, pattern recognition, Majorana, mass, double beta decay

关键词:中微子，潘达克斯三号，拓扑学，模式识别，马略纳，质量，双 β 衰变

(Some figures may appear in colour only in the online journal)

(有些数字可能只在网络日志中以彩色显示)

1.Introduction

1.介绍

The neutrino sector has been one of the most promising research areas for searching for new physics beyond the standard model (SM).Neutrino oscillations and the inferred non-zero neutrino mass offered a concrete evidence of new physics, as demonstrated by experiments including Super-Kamiokande [1], SNO [2], and etc.Early in 1937, the possibility for an electrically neutral fermion to be the anti-particle of itself was raised by Majorana [3], and neutrinos are the most promising candidates for the so-called Majorana fermions.Soon after that, physicists started to use the neutrinoless double beta decay (0νββ) to search for the existence of Majorana neutrinos [4].In a SM-allowed two-neutrino double beta decay process, two neutrons in a candidate nucleus decay into two protons simultaneously and emit two electrons together with two electron antineutrinos.Such a process has been observed in a dozen or so isotopes, including Ge, Te, Xe, and etc

中微子领域一直是寻找超越标准模型的新物理的最有前途的研究领域之一。中微子振荡和推断的非零中微子质量为新物理学提供了具体的证据，包括超级卡米诺坎德·[1 号、SNO·[2 号等的实验证明了这一点。早在 1937 年，马略纳·[3]就提出了电中性费米子成为自身反粒子的可能性，中微子是所谓的马略纳费米子最有希望的候选者。此后不久，物理学家开始使用无中微子双 β 衰变(0νββ)来寻找马略纳中微子[4]的存在。在 SM 允许的双中微子双 β 衰变过程中，候选核中的两个中子同时衰变为两个质子，并发射两个电子和两个电子反中微子。这一过程已在十几种同位素中观察到，包括锗、碲、氙等

Author to whom any correspondence should be addressed.

任何信件都应该寄给的作者。

2

(see, for example [5]).If neutrinos are Majorana fermions, no electron antineutrinos are released in the double beta decay process.It has also been argued with the Black Box theorem that an observation of 0νββ directly indicates the Majorana nature of neutrinos [6].The experimental observation of 0νββ will also distinctly violate the conservation of the lepton number, and have far-reaching impact beyond the neutrino sector [7].After about 80 years of experimental effort, no firm evidence for 0νββ has been obtained.Several major experiments are taking data or are under construction and many more smaller-scale efforts are in R&D phase.Current status and expected sensitivity can be seen in [8] and references within.

(例如，见[5)。如果中微子是 Majorana 费米子，在双 β 衰变过程中不会释放电子反中微子。也有人用黑盒定理证明，0νββ 的观测直接表明中微子的马略纳性质[6]。0νββ 的实验观察也将明显违反轻子数守恒，并对中微子扇面[7]之外有深远的影响。经过大约 80 年的实验努力，没有获得关于 0νβββ 的确凿证据。几个主要的实验正在获取数据或正在建设中，许多更小规模的努力都处于 R&D 阶段。目前的状况和预期的敏感性可以在[8]和参考文献中看到。

The PandaX-III experiment aims to search for 0νββ of Xe using a high pressure gaseous time projection chamber (TPC) [9].The experiment will be located in the newly excavated China JinPing underground Laboratory Phase II (CJPL-II) in Sichuan Province, China [10].As a calorimeter, PandaX-III measures the energy of two electrons from 0νββ and constructs an energy spectrum at

the region of interest (ROI) around the Qββ value of Xe, 2,457.83 keV [11].The expected energy resolution is better than 3% full-width-half-maximum (FWHM) at the Qββ value

PandaX-III 实验旨在使用高压气体时间投影室(TPC) [9]寻找氙的 0νββ。该实验将位于新发掘的中国[四川省中国金平地下实验室二期(CJPL 二期)。作为一种量热计，PandaX-III 从 0νβββ 测量两个电子的能量，并在 Xe 的 Qβββ 值(2457.83 keV[11)附近的感兴趣区域构建能谱。在 Qββ 值处，预期能量分辨率优于 3%全宽半最大值(FWHM)

[12, 13].PandaX-III follows the standard recipe of a low background experiment, including deep underground lab environment, passive shielding, and careful screening of detector as well as electronics material to minimize the number of dubious background events in the ROI.The descendants of U and Th, mainly Bi and Tl, contribute most significantly to the background in the ROI.One of the gamma lines from Bi at 2448 keV, only 10 keV below the 0νββ Q-value, poses a major challenge to event identification with energy alone.The expected background level at the ROI including a realistic detector response is on the order of 10−keV−kg−yr−when considering only the event energy.

[12，13]。PandaX-III 遵循低背景实验的标准配方，包括深层地下实验室环境、被动屏蔽、探测器和电子材料的仔细筛选，以尽量减少投资回报中可疑背景事件的数量。铀和钍的后代，主要是铋和铊，对投资回报率的背景贡献最大。来自铋的伽马线中的一条在 2448 千电子伏，仅比 0νββ Q 值低 10 千电子伏，对仅用能量进行事件识别构成了重大挑战。当仅考虑事件能量时，预计的感兴趣区域背景水平(包括真实的探测器响应)约为 10 千电子伏/千克年。

Additional background suppression can be realized with event tracking information, which is the main topic of this paper.Different from other detector technologies, a gaseous TPC will record detailed trajectories of the two electrons from a potential 0νββ event.PandaX-III will exploit the electron tracking potential using fine-pitched Microbulk Micromegas [14] readout planes to reach millimeter level spatial resolution, in comparison with the typical 0νββ track length of 10cm scale at 10 bar.The signal identification will exploit the features of the electron tracks topology pro-duced by 0νββ decays.The two electrons generated by a 0νββ decay will produce two bright Bragg peaks, occurring on at least 95% of the decays [15].On the other hand, gamma background events in the ROI normally have only one Bragg peak.We will review the details on the main characteristics of signal and background events, previously investigated in [15], and we will exploit them to perform a discrimination analysis to demonstrate the ultimate background level achievable by the PandaX-III setup.

事件跟踪信息可以实现额外的背景抑制，这是本文的主要内容。与其他探测器技术不同，气态 TPC 将记录来自 0νββ 事件的两个电子的详细轨迹。与 10 巴下 10 厘米尺度的典型 0νββ 轨道长度相比，PandaX-III 将利用细间距微球微兆[14]读出平面开发电子跟踪潜力，以达到毫米级空间分辨率。信号识别将利用 0νββ 衰变产生的电子轨道拓扑特征。0νββ 衰变产生的两个电子将产生两个明亮的布拉格峰，至少在 95%的衰变中出现[峰。另一方面，感兴趣区域中的伽马背景事件通常只有一个布拉格峰。我们将回顾信号和背景事件的主要特征的细节，以前在[15]中进行过研究，我们将利用它们来进行鉴别分析，以证明 PandaX-III 装置可达到的最终背景水平。

The work presented in this paper includes an accurate Monte Carlo simulation of the operation of the PandaX-III detector setup from the point of view of 0νββ event identifica-tion.Previous work, published in [9], provided a rough estimation of the final background achievable.This paper provides a complete and detailed analysis for PandaX-III including a realistic two-dimensional detector readout.

本文介绍的工作包括从 0νββ 事件识别的角度对潘达克斯三号探测器装置的操作进行精确的蒙特卡罗模拟。先前的工作，发表在[9]，提供了一个最终背景可达到的粗略估计。本文提供了一个完整和详细的分析，包括一个现实的二维探测器读数。

PandaX-III adopts the event-oriented software framework RESTfor simulation and data analysis, especially to facilitate the topological analysis.With REST and the underlying Geant4 framework, we simulate 0νββ events and background events with energy deposition and tracking information in the gas medium.Realistic detector response, including the strip readout scheme, is then added to generate mock data, which are then fed into our data analysis chain for energy and track reconstruction.We then optimize the efficiency of the

PandaX-III 采用面向事件的软件框架 RESTfor 进行仿真和数据分析，特别是为了方便拓扑分析。借助 REST 和底层 Geant4 框架，我们模拟了 0νββ 事件和背景事件，并在气体介质中记录了能量沉积和跟踪信息。然后加入真实的探测器响应，包括条带读出方案，以生成模拟数据，然后将其输入我们的数据分析链，用于能量和轨迹重建。然后我们优化的效率

We include in appendix A necessary technical details on the software used, and the description of the event data and event process routines used in our analysis.Any keyword starting by TRest will do reference to REST and it will be detailed in one of the appendices of this document.

我们在附录 A 中包括了所用软件的必要技术细节，以及我们分析中使用的事件数据和事件处理程序的描述。任何以 TRest 开头的关键字都将引用 Rest，并将在本文档的附录中详细说明。

3

discrimination between signal and background by analyzing the topological information of the events.

通过分析事件的拓扑信息来区分信号和背景。

This paper is organized as follows.In section 2 we present the results obtained in terms of signal-to-background enhancement for the PandaX-III baseline readout scheme.In section 3, we explore the impact of different readout granularities and assess the goodness of choice for the PandaX-III baseline readout.Finally, in section 4, we go a step forward in our analysis to demonstrate the capability of our detector to fiducialize in the drift direction of the TPC and reject background from our charge readout plane effectively.

本文组织如下。在第二部分中，我们介绍了根据 PandaX-III 基线读出方案的信号-背景增强而获得的结果。在第三节中，我们探讨了不同读出粒度的影响，并评估了 PandaX-III 基线读出的选择优度。最后，在第 4 节中，我们在分析中向前迈进了一步，展示了我们的检测器能够在 TPC 的漂移方向上实现基准化，并有效地抑制电荷读出平面的背景。

2.Background rejection on the PandaX-III baseline readout scheme

2.PandaX-iii 基线读出方案的背景抑制

We present here the results obtained using a realistic detector readout description based on the existing PandaX-III baseline Microbulk Micromegas design [16].For the sake of com-pleteness, we provide in appendix B details on how we generate our Monte Carlo event data including any necessary details such as physics considerations and detailed detector readout description for PandaX-III, based on a two-dimensional charge readout, which represents a major milestone on the event reconstruction and data analysis of the experiment.In section 2.1, we define the parameters, extracted during the event data processing, that will be used for event pattern recognition, leading to our final background discrimination results reported in section 2.2.

我们在此展示了基于现有的 PandaX-III 基线微弹道导弹设计[16]的现实探测器读出描述所获得的结果。为了完整起见，我们在附录 B 中提供了我们如何生成蒙特卡罗事件数据的详细信息，包括任何必要的细节，例如基于二维电荷读出的物理考虑和详细的探测器读出描述，这是事件重建和实验数据分析的一个重要里程碑。在第 2.1 节中，我们定义了在事件数据处理过程中提取的参数，这些参数将用于事件模式识别，从而得出第 2.2 节中报告的最终背景辨别结果。

2.1.Topological parameters used for pattern recognition

2.1 .用于模式识别的拓扑参数

This section does not focus on the nature, or the source, of background events, but mostly on the type of background events that might mimic a 0νββ in the ROI at the Qββ energy of Xe.Such background events, producing a topological structure similar to a 0νββ decay, can only be produced in the active detector volume by gammas with an energy equal to or above the Qββ value.Some of those gammas end up producing a long electron track of characteristics similar to the 0νββ signal.Still, a good choice of parameters extracted from the physical track provides an excellent instrument to differentiate between this kind of events and electron tracks produced by 0νββ decays.

本节不关注背景事件的性质或来源，但主要关注背景事件的类型，这些背景事件可能在 Xe 的 Qββ 能量下模拟投资回报率中的 0νββ。这种产生类似于 0νββ 衰变的拓扑结构的背景事件，只能由能量等于或高于 Qββ 值的 γ 在活动探测器体积中产生。其中一些伽马射线最终会产生一个特征类似于 0νββ 信号的长电子轨迹。尽管如此，从物理轨道提取的参数的良好选择提供了区分这种事件和由 0νββ 衰变产生的电子轨道的极好工具。

Previous studies on 0νββ pattern recognition [1719] have already shown the potential of certain parameters, such as the number of secondary tracks or end-track energies to differentiate background and signal events.We reach the same conclusions, and we obtain comparable results on their discrimination power.Furthermore, we will investigate the potential of novel parameters never used in previous studies, viz.as the end-track twist parameter and the track length.Below we discuss the respective merits of both, previously mentioned and novel parameters.

先前对 0νββ 模式识别的研究[1719]已经显示了某些参数的潜力，例如次级轨道的数量或末端轨道能量来区分背景和信号事件。我们得出了相同的结论，并且在它们的辨别能力上获得了可比较的结果。此外，我们将研究以前研究中从未使用过的新参数的潜力，即。作为结束轨道扭曲参数和轨道长度。下面我们讨论两者各自的优点，前面提到的和新颖的参数。

• Number of secondary tracks, or track energy ratio.One of the most powerful discriminators is related to the number of independent tracks identified inside an event taking place in the active detector volume.Background events are originated by high energy gammas, and many of those gammas interacting in the detector will produce multi-track events due to Compton scattering combined with a photoelectric interaction absorbing the remaining gamma energy, therefore producing a main long energetic track.Additionally, the higher initial energy of the single electron background compared to the

次要轨道的数量或轨道能量比。最强有力的鉴别器之一与在活动探测器体积中发生的事件内部识别的独立轨迹的数量有关。背景事件是由高能伽马射线引起的，由于康普顿散射与吸收剩余伽马射线能量的光电相互作用相结合，许多在探测器中相互作用的伽马射线将产生多道事件，从而产生主要的长能量轨道。此外，与单电子背景相比，单电子背景的初始能量越高

The number of tracks is found after using TRestHitsToTrackProcess, described in appendix A.2, while the conditions in which those are obtained is described in appendix B.1.

如附录 A.2 所述，在使用 TRestHitsToTrackProcess 后，可找到磁道数，而获得这些磁道的条件如附录 B.1 所述

4

initial energy of each of the two electrons generated in the 0νββ decay makes so that the probability of producing secondary gamma radiation is higher for single electron background events.

在 0νββ 衰变中产生的两个电子的每一个的初始能量使得对于单个电子背景事件产生次级伽马辐射的概率更高。

In practice, it is convenient to define the track energy ratio, θ, as the ratio between the total energy of secondary tracks and the total energy of the event, Etot, expressed as

在实践中，将径迹能量比 θ 定义为次级径迹总能量与事件总能量 Etot 之比是方便的，表示为

q = å E = E n N i n tot 1 i i

q = E = E N N I N 总计 1 i i

( )

( )

where Ei, n is the energy of track number n from projection i, and ni = 0 corresponds to the most energetic track of each projection.If the event does not contain secondary tracks, as it is frequently the case in 0νββ events, the value of θ will be zero.Such a definition accommodates the 2D and 3D detector readouts in a single observable, and provides a probability density function of the θ parameter that can be exploited for signal and background separation.It is important to remark that the definition of θ is done for convenience on the flexibility to tune the signal-to-background ratio by selecting an appropriate θ-value.We have compared ourselves this observable with other approaches used in other studies [17], obtaining very similar results.It must be remarked, that using the θ parameter does not constrain the number of tracks.However, typically low values of θ will accept mostly events containing only one or two tracks, and rarely three.

其中，Ei，n 是来自投影 I 的轨道号 n 的能量，并且 ni = 0 对应于每个投影的最大能量轨道。如果事件不包含次要轨迹，如 0νββ 事件中经常出现的情况，θ 的值将为零。这种定义将 2D 和 3D 探测器读数容纳在单个可观测值中，并提供 θ 参数的概率密度函数，可用于信号和背景分离。需要注意的是，θ 的定义是

为了方便灵活地通过选择合适的 θ 值来调整信号与背景的比率。我们将自己的这一观察结果与[其他研究中使用的其他方法进行了比较，获得了非常相似的结果。必须指出，使用 θ 参数并不限制轨道数量。然而，通常 θ 值较低的情况下，大多数事件只包含一个或两个轨迹，很少包含三个轨迹。

• End-track energies, or blobs charge.An electron traveling in a gas medium with energies above ∼MeV experiences a constant energy loss, dE/dx, along its trajectory in the medium.Once the electron loses most of its energy, at levels well below 1 MeV, its dE/dx increases suddenly until it loses all of its kinematic energy.This phenomenon produces a high density charge region at the electron track end, or Bragg peak, commonly called blob.Obviously, a 0νββ track emitting two electrons with a common origin will be similar to a single track with two blobs at the track ends, while single electron background tracks will only produce one Bragg peak.The end of single electron tracks where no blob is found will be called tail.

末端轨道能量或斑点电荷。能量在 MeV 以上的气体介质中运行的电子，沿其在介质中的轨迹会经历一个恒定的能量损失，dE/dx。一旦电子失去大部分能量，在 1 MeV 以下，它的 dE/dx 会突然增加，直到失去所有动能。这种现象在电子轨道末端产生高密度电荷区，或称布拉格峰，通常称为斑点。显然，发射两个具有共同原点的电子的 0νββ 轨道将类似于在轨道末端具有两个斑点的单个轨道，而单个电子背景轨道将仅产生一个布拉格峰。没有发现斑点的单电子轨道的末端将被称为尾部。

The energy, or charge, , in a certain blob is determined by summing up the energy deposited around a sphere of radius Ro centered at each of the high density track end coordinates.The following mathematical expression summarizes our blob charge definition

某个斑点中的能量或电荷⌧是通过将以每个高密度轨道末端坐标为中心的半径为 Ro 的球体周围沉积的能量相加来确定的。下面的数学表达式总结了我们的斑点电荷定义

= = å ( ) ()

= =()

= <

= <

j q and min , , 2

·j·q 和敏，2

dr R

博士

n l 1 2

n l 1 2

jn o ,

jn o，

where the index j = 1, 2 represents each of the track ends, and the index n corresponds to the hit number inside the TRestTrackEvent definition (given in appendix A).The charge integration at each

end-track, 1,2, is performed for those hits, qn, that satisfy that the hit distance d to the blob coordinates, at each track end, j, is below Ro.Different combinations of 1 and 2 may be chosen to construct an observable to be used for pattern recognition.In our posterior analysis we will use the lowest charge blob definition, l, a value which, in principle, is necessarily low for background events in which the electron tail is properly identified, while for 0νββ events cannot be low.In the case of two-dimensional readouts this observable is independently calculated for each projection, obtaining two values, l X and l Y , to be combined later.

其中，索引 j = 1，2 代表每个轨道末端，索引 n 对应于 TRestTrackEvent 定义中的命中数(在附录 A 中给出)。对于满足在每个轨道末端 j 到斑点坐标的命中距离 d 低于 Ro 的那些命中 qn，在每个末端轨道 ⍁1,2 处执行电荷积分。可以选择⍁1 和⍁2 的不同组合来构建用于模式识别的可观测值。在我们的后验分析中，我们将使用最低电荷斑点定义，⍁l，这个值原则上对于电子尾被正确识别的背景事件来说必然是低的，而对于 0νββ 事件来说不可能是低的。在二维读出的情况下，对于每个投影独立地计算这种可观测性，获得两个值，⍁l X 和⍁l Y，稍后进行组合。

• End-track twist.Another feature characterizing the behavior of the electron trajectory near the blob is the erratic nature of its trajectory.This erratic behavior, due to higher electron

端轨扭曲。表征斑点附近电子轨迹行为的另一个特征是其轨迹的不稳定性。这种不稳定的行为，是由于更高的电子

The blob coordinates are obtained by TRestFindTrackBlobsProcess, detailed in appendix B.3.

斑点坐标由 TRestFindTrackBlobsProcess 获得，详见附录 B.3

5

scattering angles, does not manifest at the initial interaction vertex, or tail, at single electron background events.On the contrary, energetic electrons, with initial energies of the order of the Qββ value, will usually produce a clear straight tail.In order to quantify this effect we introduce the twist parameter that measures the angle between consecutive hits belonging to a top-level tracknear the track ends.The twist parameter, ξ, is expressed as follows

散射角在单电子背景事件的初始相互作用顶点或尾部不明显。相反，初始能量为 Qββ 值的高能电子通常会产生清晰的直尾。为了量化这种影响，我们引入了扭曲参数，该参数测量在轨道末端附近属于顶级轨道的连续命中之间的角度。扭曲参数 ξ 表示如下

x =- = å(ˆ ˆ) ( ) ()

x =-= 0(˘˘)()

=

=

+ N n n

+N N N N

1 2, and min , , 3 j

1 2，最小，3 j

j i

j i

N

N

i i

我

0

0

1

1

j

j

x xx l 1 2

x xx l 1 2

where nˆi represents the unit vector defined by the ith and ith 1 + nodes of a reconstructed top-level track, and i = 0 can be identified with the first (or last) node of the physical track.The total number of hits, Nj, considered in each end-track, j = 1, 2, is relative to the total number of hits, Ntot, at the top-level track.In our analysis we have defined Nj as the 25% of Ntot, i.e. a track containing Ntot = 28 hits will average the 6 angles formed by the 7 hits closer to the end-tracks.The normalization factor 2 in the previous expression is introduced to assure ξ is mathematically contained in the range (0, 1), where ξ = 0 means that the nodes are fully aligned.As in the previous observable, we define ξl as the lowest value between the twist parameter obtained at each end-track, and obtain independent values for each projection, xl X and xl Y , for the two-dimensional case.

其中 nˆ i 表示由重构的顶层轨道的第 I 个和第 I 个+节点定义的单位向量，i = 0 可以用物理轨道的第一个(或最后一个)节点来标识。在每一个结束轨道中考虑的总命中数 Nj = 1，2，是相对于顶层轨道的总命中数 Ntot。在我们的分析中，我们已经将 Nj 定义为 Ntot 的 25%，也就是说，包含 Ntot = 28 次命中的轨迹将平均 7 次命中形成的 6 个角度更接近末端轨迹。前面表达式中的归一化因子 2 被引入，以确保 ξ 在数学上包含在范围(0，1)中，其中 ξ = 0 表示节点完全对齐。如前所述，我们将 ξl 定义为在每个末端轨迹获得的扭曲参数之间的最小值，并获得二维情况下每个投影的独立值，xl X 和 xl Y。

• Track length.We might also expect that two electron 0νββ tracks will produce a slightly shorter path due to the generation of two blobs, and therefore a higher dE/dx in average.Although this observable is expected to have a weak discriminating power, we still assess its performance.

轨道长度。我们也可以预期，由于两个斑点的产生，两个电子 0νββ 轨道将产生稍微更短的路径，因此平均具有更高的 dE/dx。尽管这种可观察到的现象被认为具有微弱的辨别能力，我们仍然评估它的性能。

The track length, , is simply calculated as the total measured distance between the track ends, following the ordered node sequence at the top-level track produced after TRestTrackReconnectionProcess.Expressed as

轨道长度⌧简单地计算为轨道末端之间的总测量距离，遵循在 tresttrackreconnectionprocess 之后产生的顶层轨道的有序节点序列。表示为

= å

= a

=

=

-

-

d + , 4

d +，4

i

i

N

N

i i

我

0

0

1

1

, 1

，1

( )

( )

where N is the total number of hits, or nodes, in the top-level track, and di i, 1 + is the distance between the hit i and i + 1, or connected hits.Again, for the two-dimensional case we will obtain 2 independent length measurements for each projection, X and Y .

其中，N 是顶级曲目中的点击数或节点总数，di i，1 +是点击数 I 和 i + 1 或连接点击数之间的距离。同样，对于二维情况，我们将为每个投影获得两个独立的长度测量值，⊠X 和⊠Y。

In summary, these observables will allow us to discriminate background by differ-entiating the main background and signal properties.When identifying a 0νββ signal event we search for a main energetic track, with almost negligible energy deposition on secondary tracks belonging to the event.Signal events will generally lack the presence of an end-track tail, and therefore, the combination of low end-track values for blob charge, l and twist parameter, ξl, will be decisive on the identification of such a feature.These main char-acteristics can be easily recognized on the background and signal events shown in figure B3, at appendix B.

总之，这些可观察到的现象将允许我们通过区分主要的背景和信号特性来辨别背景。当识别一个 0νββ 信号事件时，我们寻找一个主能量轨道，在属于该事件的次轨道上几乎可以忽略能量沉积。信号事件通常不存在末端轨迹尾部，因此，斑点电荷、⊠l 和扭曲参数 ξl 的低端轨迹值的组合将对这种特征的识别起决定性作用。这些主要特征可以很容易地在背景和信号事件上识别，如图 B3 附录 b 所示

Finally, it is important to remark that these parameters serve also to describe in a quantitative way each event, i.e. they can be exploited to characterize the experimental data and support the construction of a Monte Carlo background model.The nature from different background contributions due to the different contamination sources and components in the detector might be better understood by studying the behavior of these parameters on different

最后，重要的是注意到这些参数也用于以定量的方式描述每个事件，即它们可以被用来表征实验数据并支持蒙特卡罗背景模型的构建。通过研究这些参数在不同环境中的行为，可以更好地理解由于不同的污染源和检测器中的成分而产生的不同背景贡献的性质

A top-level track in our analysis identifies with the physical track reconstructed, see also TRestTrackEvent definition at appendix A,

我们分析中的顶级轨道与重建的物理轨道一致，另请参见附录 A 中的 TRestTrackEvent 定义。

6

populations of events, measured at different data taking conditions.Therefore, even if a parameter does not contribute finally on the signal-to-background significance, it may be valuable in other scenarios to help understanding the nature of the data collected with the detector.

在不同的数据采集条件下测量的事件总数。因此，即使某个参数最终没有对信号至背景的重要性做出贡献，在其他情况下，它也可能有助于了解检测器收集的数据的性质。

2.2.Results

2.2 .结果

We report in this section the results obtained on background reduction considering the topological features of signal and background events.We will take into account the forecasted PandaX-III data taking conditions, i.e. a vessel filled with 10 bar of xenon+TMA 1% gas mixture, and a detailed detector response, carefully described in appendix B.

我们在本节中报告了在考虑信号和背景事件的拓扑特征的情况下，背景缩减所获得的结果。我们将考虑预测的 PandaX-III 数据采集条件，即一个装有 10 巴氙+TMA 1%气体混合物的容器，以及详细的探测器响应，详见附录 B

The Monte Carlo 0νββ signal events, used to define our signal efficiency have been imported in RestG4 using a Decay0 [20] pre-generated event population.The initial 4-momentum definition of each of the two electrons produced by the 0νββ decay is randomly positioned at the active volume of the detector, or gas volume, for each event, and then tracked using Geant4 physics processes.

蒙特卡洛 0νββ 信号事件，用于定义我们的信号效率，已使用十进制[20]预生成的事件总体导入 RestG4。对于每个事件，由 0νββ 衰变产生的两个电子中的每一个的初始 4 动量定义被随机地定位在探测器的有效体积或气体体积，然后使用 Geant4 物理过程进行跟踪。

In [9], the main contamination sources contributing to the background of the experiment were analyzed, allowing to identify the most critical detector components in terms of negative impact to the overall background of the experiment.In this work we go a step further by presenting a more definite background level achievable with the PandaX-III detector.For that purpose, we have chosen representative detector components, as the high pressure copper vessel and the Micromegas readout plane, to evaluate the pattern recognition capability of our event reconstruction algorithms.We have simulated the U and Th decay chains at those detector components.For the copper vessel we generate our events randomly on the bulk of the material, while for the Micromegas contamination we generate surface events at the readout plane location, behind 10µm of copper.In order to guarantee enough statistics at the end of our topological analysis we have generated near 10decays of U and Th isotopes for the vessel contribution, and 5 × 10decays for the Micromegas contributions.Our signal efficiency has been calculated over an initial population of 10generated 0νββ events.

在[9]中，分析了造成实验背景的主要污染源，从而能够根据对实验整体背景的负面影响来确定最关键的检测器组件。在这项工作中，我们更进一步，提出了一个更明确的背景水平可实现的潘达克斯三型探测器。为此，我们选择了有代表性的探测器组件，如高压铜容器和微兆读出平面，来评估我们的事件重建算法的模式识别能力。我们已经模拟了这些探测器组件上的铀和钍衰变链。对于铜容器，我们在大部分材料上随机产生我们的事件，而对于微兆污染，我们在 10µm 铜后面的读出平面位置产生表面事件。为了保证在拓扑分析结束时有足够的统计数据，我们已经为容器贡献生成了近 10 倍的铀和钍同位素，为微兆贡献生成了 5×10 倍的铀和钍同位素。我们的信号效率是在 10 个生成的 0νββ 事件的初始总体上计算的。

Signal and background events have been processed following the scheme described in appendix B.1. Figure 1 shows the parameter distributions obtained during the data processing chain, and described previously on section 2.1.Except for the track energy ratio, it must be noted that the other distributions follow similar patterns for different simulated background components.

信号和背景事件已经按照附录 B.1 中描述的方案进行了处理。图 1 显示了在数据处理链中获得的参数分布，如前面第 2.1 节所述。除了轨道能量比之外，必须注意的是，对于不同的模拟背景分量，其他分布遵循相似的模式。

We apply our criteria to discriminate signal from background sequentially on these parameters, following the order given in the list provided in section 2.1.We combine the XZ-and YZ-projections into a single parameter by choosing the minimum value of each projection for the blob charge, min , and twist parameter, xmin , i.e. for each event we only consider the two-dimensional projection where tail identification is more obvious.While we have chosen the maximum track length of each projection, max , supported by the argument that 0νββ events are expected to be shorter.We have obtained our threshold values, or cuts, such that they maximize the signal-to-background significance by maximizing the figure of merit, s b , at each of the four topological criteria used in our analysis, i.e. track energy ratio, blob charge, twist parameter and track length.Here, òs and òb correspond to the signal and background reduction factors at each of those steps.The following topological parameter conditions were obtained after such optimization

我们应用我们的标准，按照第 2.1 节列表中给出的顺序，在这些参数上依次区分信号和背景。我们通过选择斑点 charge, min 和扭曲参数 xmin 的每个投影的最小值，将 XZ 和 YZ 投影组合成单个参数，即对于每个事件，我们只考虑尾部识别更明显的二维投影。虽然我们选择了每个投影的最大轨道长度，但 max 支持 0νββ 事件预计会更短的论点。我们已经获得了我们的阈值或切割，从而通过在我们分析中使用的四个拓扑标准(即轨道能量比、斑点电荷、扭曲参数和轨道长度)中的每一个上最大化品质因数 s·b· ，使信号与背景的显著性最大化。这里的“s”和“b”对应于每个步骤中的信号和背景降低因子。优化后得到以下拓扑参数条件

q ·

q

x

x

< >

< >

> <

> <

2.66 10 , 160 keV

2.66 10，160 千电子伏

0.008 and 204 mm.

0.008 和 204 毫米

l

l

l

l

3 min

3 分钟

min max

最小最大值

7

7

J.Phys. G: Nucl.Part.Phys. 47 (2020) 045108 J Galan et al

J.物理 G: Nucl。部分。《物理》47 (2020) 045108 J Galan 等人

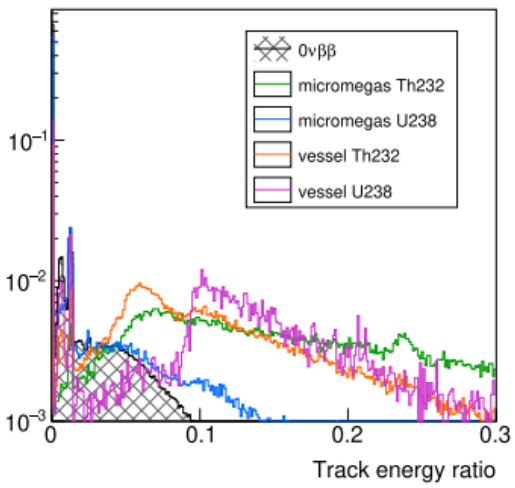

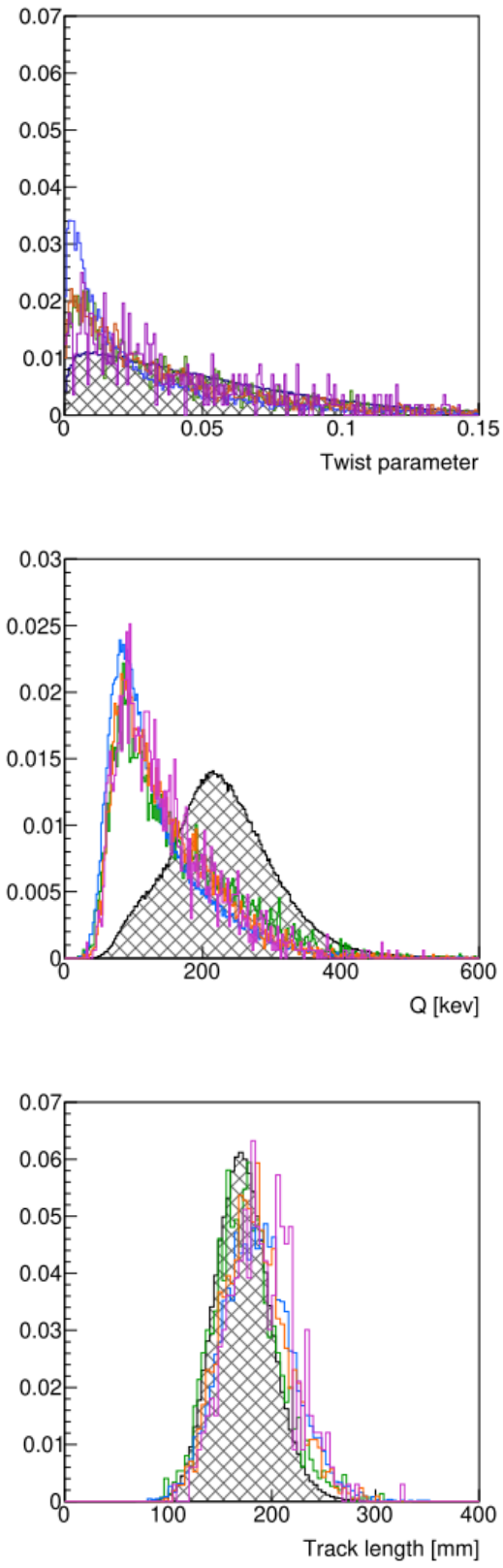

Figure 1.The distributions of topological parameters, normalized to unity, obtained from the XZ-projection of 0νββ event tracks (filled curve), compared to the equivalent distributions of the four background datasets considered in our study (colored curves).The distributions are built using only the events contained in the ROI, i.e. in the energy range (2395, 2520) keV.On top of that, each distribution accumulates the sequential topological criteria we applied in the preceding parameter. (a) The track energy ratio, or θ parameter.Different physics processes contribute to create certain structures on this distribution.Peaks found at low θ-values, θ 0.01, are related to the escape peaks

of xenon, while hills appearing at higher values are related to bremsstrahlung gamma emission produced by high energy electron tracks, or Compton scattering processes that end up on a photoelectric process producing a main electron energetic track.(b) The lower track energy blob, l X . Events satisfying θ < 1.33 × 10−.(c) The lower twist parameter, xl X, satisfying θ < 1.33 × 10−and l > 176 X keV.(d) The track length, X, satisfying θ < 1.33 × 10−, l > 176 X keV and x > 0.0133 l X .

图 1。与我们研究中考虑的四个背景数据集(彩色曲线)的等效分布相比，从 0νββ 事件轨迹(填充曲线)的 XZ 投影获得的归一化为 1 的拓扑参数分布。分布仅使用投资回报中包含的事件构建，即在能量范围 (2395，2520) keV 内。最重要的是，每个分布都累积了我们在前面的参数中应用的连续拓扑标准。轨道能量比或 θ 参数。不同的物理过程促成了这种分布的某些结构。在低 θ 值 θ 0.01 处发现的峰与氩的逃逸峰有关，而在较高值处出现的峰与高能电子轨道或康普顿散射过程产生的韧致辐射 γ 发射有关，康普顿散射过程以产生主电子能量轨道的光电过程结束。(b)满足 θ < 1.33 × 10 的较低轨道能量斑点，⊠l X 事件。(c)较低的扭转参数 xl X，满足 θ < 1.33 × 10，⊠l > 176×kev。(d)轨道长度，⊠X，满足 θ < 1.33 × 10，⊠l > 176×kev，x > 0.0133 l×x。

The final selected event population, signal or background events, will necessarily satisfy those conditions.We should mention that these values have been obtained by optimizing the dataset corresponding to the U vessel generated events.However, it must be noted that such a choice is not critical in view of the similar behavior of the different topological

最终选定的事件群体、信号或背景事件将必然满足这些条件。我们应该提到，这些值是通过优化对应于美国船只生成事件的数据集获得的。然而，必须注意的是，鉴于不同拓扑的相似行为，这样的选择并不重要

8

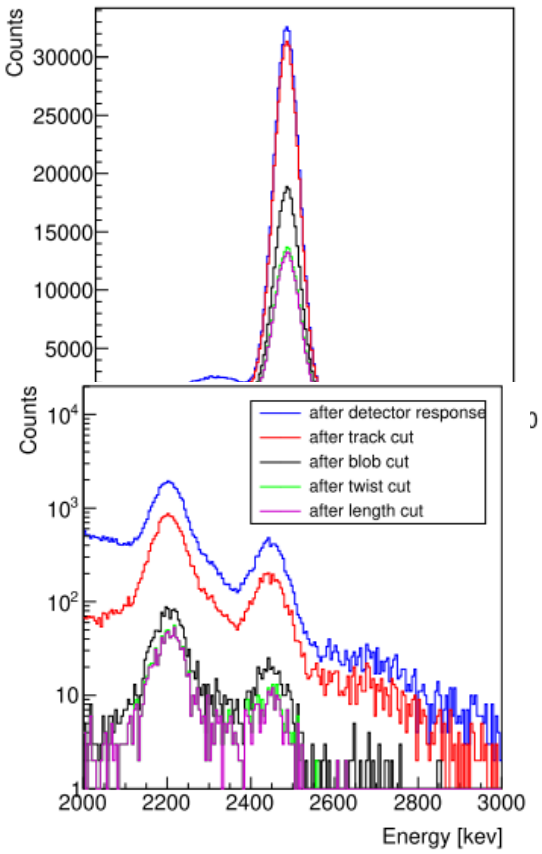

Figure 2.(a) The simulated energy spectrum response of 0νββ events around the Qββ value, and the resulting spectra after applying the different topological criteria sequentially, i.e. track energy ratio, blob charge, twist parameter and track length.The main peak corresponds to 0νββ events for which full decay energy was acquired by our detector, while the distribution left tail corresponds to 0νββ events with partial energy loss outside the detector readout plane boundaries, or partially contained in the detector acquisition window, limited by the electronics.(b) The equivalent background spectra

图 2 .(a)围绕 Qββ 值的 0νββ 事件的模拟能谱响应，以及顺序应用不同拓扑标准(即轨道能量比、斑点电荷、扭曲参数和轨道长度)后的结果谱。主峰对应于 0νββ 事件，对于该事件，我们的检测器获得了全部衰减能量，而左尾分布对应于 0νββ 事件，其部分能量损失在检测器读出平面边界之外，或者部分包含在受电子器件限制的检测器获取窗口中。等效背景光谱

resulting from U decays generated from the copper vessel.The peaks observed correspond to two high energy gammas, 2204 and 2448 keV, from the spectrum gamma emission of Bi present in the U decay chain.The 3% FWHM Gaussian smearing introduced by the TRestHitsSmearingProcess can be recognized in both figures.

由铜容器产生的铀衰变产生。观察到的峰值对应于两个高能 γ，2204 和 2448 千电子伏，来自铀衰变链中铋的能谱 γ 发射。在这两个图中，都可以识别出由特雷斯脱测量过程引入的 3% FWHM 高斯拖尾。

parameters produced by different background sources and components, as it can be observed in figure 1.As a consequence, the threshold values obtained are not strongly dependent on this choice.Anyhow, we must remark that the most sensitive threshold value corresponds to the track energy ratio parameter, as it can be induced from the distribution presented in figure 1(a).Anyhow, in our particular conditions, we observe that the low value of θ, resulting in our particular optimization, constrains our event selection practically to the population of events that contain only one single main track.

由不同的背景源和成分产生的参数，如图 1 所示。因此，获得的阈值并不强烈依赖于这种选择。无论如何，我们必须注意，最敏感的阈值对应于轨道能量比参数，因为它可以从图 1(a)所示的分布中导出。总之，在我们的特定条件下，我们观察到 θ 的低值导致了我们的特定优化，实际上将我们的事件选择限制在只包含一个主轨迹的事件总体上。

Before applying the sequential topological criteria we filter the event population to those events that are found in the ROI, defined as Qββ σ, where σ = 31 keV is given by the assumed 3% FWHM energy resolution, introduced in TRestHitsSmearingProcess (see appendix A.2).

在应用顺序拓扑标准之前，我们将事件群体过滤到那些在投资回报中发现的事件，定义为 Qββ σ，其中 σ = 31 keV 是由假设的 3% FWHM 能量分辨率给出的，引入到投资回报度量过程中(见附录 A.2)。

The energy definition considered is the value extracted from TRestTriggerAnalysisPro-cess (see appendix B.3) which contains all the effects introduced by the detector readout response.The resulting energy spectrum for 0νββ, together with one of the background components studied is shown in figure 2, including the accumulated effect of sequential cuts on signal efficiency and background reduction.

所考虑的能量定义是从 TRestTriggerAnalysisPro 过程(见附录 B.3)中提取的值，该过程包含由探测器读出响应引入的所有影响。图 2 显示了 0νββ 的最终能谱以及所研究的一个背景成分，包括连续切割对信号效率和背景降低的累积影响。

Table 1 shows the percentage of accepted signal events and background reduction fac-tors, i.e. the final number of events surviving after each cut per simulated one.The first row, Geant4, is the

calorimetric response where we consider all the energy depositions in our active volume, here we only integrate events inside our ROI;the second row, Response, corresponds to the population of events that remain in the ROI after applying the detector

表 1 显示了可接受的信号事件和背景减少因子的百分比，即每个模拟事件在每次切割后幸存的最终事件数。第一行，Geant4，是量热响应，其中我们考虑了我们活动体积中的所有能量沉积，这里我们只整合了我们投资回报中的事件；第二行“响应”对应于应用检测器后仍保留在投资回报中的事件总数

9

Table 1.Percentage of accepted Xe signal events, or signal efficiency, together with the absolute background reduction factors at the ROI for the PandaX-III CDR baseline readout, after applying the detector response and sequential topological cuts described in the text.Each row includes the accumulative reduction of all previous cuts.For the sake of simplicity we avoid to express statistical errors in this table, although we will propagate them in table 2, where final background rates are given.Systematic errors related to the Geant4 generator were studied previously in [9] using two independent Monte Carlo generators and geometry implementations.Any other source of uncertainty will be discussed in our conclusions.

表 1 在应用检测器响应和本文所述的连续拓扑切割后，接受的 Xe 信号事件百分比或信号效率，以及 PandaX-III CDR 基线读数的绝对背景降低因子。每一行都包括所有先前切削的累计减少量。为了简单起见，我们避免在此表中表达统计误差，尽管我们将在表 2 中传播它们，其中给出了最终的背景比率。与 Geant4 发生器相关的系统误差先前在[9]中使用两个独立的蒙特卡罗发生器和几何实现进行了研究。不确定性的任何其他来源将在我们的结论中讨论。

Origin

起源

Gas

气体

volume Lateral vessel Micromegas

体积侧脉管微兆

Isotope

同位素

Xe

元素氙的符号

(%) U Th U Th

(%) U Th U Th

Geant4 71.1 2.28 × 10−2.10 × 10−2.69 × 10−3.38 × 10−

geant 4 71.1 2.28×10 2.10×10 2.69×10 3.38×10

Response 52.6 7.40 × 10−8.87 × 10−1.65 × 10−1.56 × 10−

响应 52.6 7.40×10 8.87×10 1.65×10 1.56×10

Track 37.7 1.71 × 10−1.13 × 10−9.60 × 10−1.14 × 10−

轨道 37.7 1.71×10 1.13×10 9.60×10 1.14×10

Blob 26.4 2.60 × 10−1.60 × 10−9.28 × 10−2.71 × 10−

斑点 26.4 2.60×10 1.60×10 9.28×10 2.71×10

Twist 22.0 1.64 × 10−1.03 × 10−4.87 × 10−1.97 × 10−

扭转 22.0 1.64×10 1.03×10 4.87×10 1.97×10

Length 17.5 7.85 × 10−6.07 × 10−3.06 × 10−1.43 × 10−

长度 17.5 7.85×10 6.07×10 3.06×10 1.43×10

response, i.e. after applying readout fiducialization and boundaries imposed by the electronics acquisition window.We should remark, that when considering background events with energies above the ROI, they may finally get inside the ROI definition due to the partial event energy registered by our detector.The subsequent rows in the table show the accumulative effect of the topological cuts applied there after.The resulting topological selection contains only contributions from the Tl isotope decay produced inside the Th decay chain, and 214Bi produced inside the 238U chain.

响应，即在应用读出基准化和电子采集窗口施加的边界之后。我们应该注意，当考虑能量高于投资回报的背景事件时，由于我们的检测器记录的部分事件能量，它们可能最终进入投资回报定义。表中的后续行显示了其后应用的拓扑切割的累积效果。最终的拓扑选择只包含钍衰变链内产生的铊同位素衰变和 238 铀链内产生的 214 铋的贡献。

We discover looking into table 1 that the topological background reduction is about a factor 100, and it is comparable for all the background components except for the U Micromegas dataset, which is worse by about a factor 2.This result is explained mainly due to the failure of our topological cuts to discriminate surface events, as revealed by figure 3(a).The surface background contamination originated from the Micromegas readout is related to Bi decays producing β-tracks emanating from the readout plane.The Bi decay is the only isotope, inside the U decay chain, producing a β-decay with Qβ end-point energy above our ROI.The surface contamination coming from the Th Micromegas decays is also present, but as it is observed in figure 3(b), there is also an important volume component which is due to a 2614 keV gamma which is produced at practically each Tl decay in the Th chain.The volume component due to Bi in the Micromegas is negligible, compared to its surface contribution, related to the fact that only about 1.5% of the decays produce a 2447 keV gamma.

我们在表 1 中发现，拓扑背景约减少了 100 倍，除了 U Micromegas 数据集之外，所有背景成分的拓扑背景约减少了 2 倍。如图 3(a)所示，这个结果主要是由于我们的拓扑切割不能区分表面事件。源自微兆读出的表面背景污染与产生从读出平面发出的 β 轨道的铋衰变有关。铋衰变是铀衰变链中唯一的同位素，产生 β 衰变，其 β 端点能量高于我们的投资回报率。还存在来自 Th 微兆衰变的表面污染，但是如图 3(b)所示，还有一个重要的体积成分，这是由于在 Th 链中几乎每个 Tl 衰变产生的 2614 keV。与表面贡献相比，微兆中由铋引起的体积分量可以忽略不计，这与只有约 1.5%的衰变产生 2447 keV 的事实有关。

Table 2 shows the final background contribution of the detector components studied, after renormalization with the corresponding material activities of U and Th for Micromegas and vessel components.We use the same values as reported in [9].The surface contamination upper limit of Micromegas being <45 nBq cm−and <14 nBq cm−, and the radiopure copper vessel bulk contamination being 0.75 μBq kg−and 0.2 μBq kg−[21], for U and Th, respectively.

表 2 显示了所研究的探测器组件的最终背景贡献，在用相应的微兆和容器组件的铀和钍的物质活动进行重整化之后。我们使用[9]中报告的相同值。对于铀和钍，微兆的表面污染上限分别为< 45 毫微克/厘米和< 14 毫微克/厘米，辐射铜容器整体污染的上限分别为 0.75 微微克/千克和 0.2 微微克/千克[21]。

We conclude that the vessel contamination contribution is negligible compared to the contribution of the Micromegas readout plane, being its estimated overall contribution at the level of 1 cpy.Of course, the final value will ultimately depend on the real surface

我们的结论是，与 Micromegas 读出平面的贡献相比，容器污染的贡献可以忽略不计，因为它的估计总贡献为 1 cpy。当然，最终值最终将取决于真实表面

10

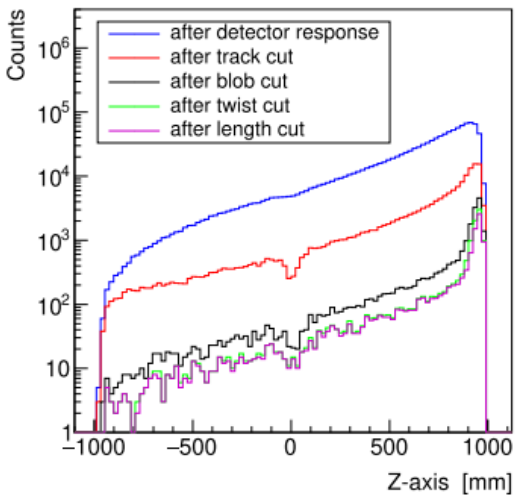

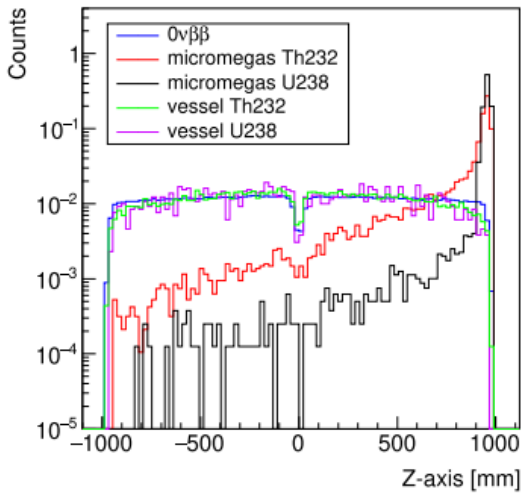

Figure 3.(a) The distribution of the average z-position for tracks from Th generated events originated from the Micromegas readout plane, placed at z = 1000 mm, after different steps of the topological cuts.(b) The distribution of the average z-position for signal and the four background contributions studied, after all the topological cuts have been applied.

图 3 .(a)在拓扑切割的不同步骤之后，位于 z = 1000 毫米的微兆读出平面产生的事件的轨道的平均 z 位置的分布。在应用所有拓扑切割之后，信号的平均 z 位置分布和所研究的四个背景贡献。

Table 2.Final background contribution after applying all the topological cuts, i.e.

表 2 应用所有拓扑切割后的最终背景贡献，即

renormalizing the results of the last row presented on table 1 using the expected Th and U isotope contamination for the different detector components.The results are

使用不同探测器组件的预期钍和铀同位素污染，对表 1 中最后一行的结果进行重正化。结果是

presented in the usual units, counts per year (top row) and keV−kg−yr−(bottom row).Measurements of microbulk Micromegas surface contamination provide results within the sensitivity limit of the measuring device, and therefore, our result for this component is given as an upper limit of the final background contribution to the experiment.

以常用单位表示，每年的计数(上一行)和 KeV kg yer(下一行)。microbulk Micromegas 表面污染的测量结果在测量设备的灵敏度极限内，因此，我们对该组件的结果作为实验的最终背景贡献的上限给出。

Lateral vessel Micromegas Units 238U 232Th 238U 232Th 6 1 13 1 < 1534 < 223 10−cpy 0.365 0.042 0.752 0.032 < 310 < 45.0 10−keV−kg−yr−

横向容器微兆单位 238 u 232 th 238 u 232 th 6 1 13 1 < 1534 < 223 10 cpy 0.365 0.042 0.752 0.032 < 310 < 45.0 10 keV kg 年

contamination present at the Micromegas readout.Considering that the contamination levels used in our Monte Carlo are limits obtained experimentally we may still remain optimistic about this contribution.In section 4 we will show how we can achieve an additional reduction on the surface contamination near the readout planes by exploiting the effect of electron diffusion on the time signals registered by our TPC [13].Finally, we must also consider our result as conservative from

the point of view that there will be probably room for improvement by enhancing the existing parameter correlations, e.g. exploiting more sophisticated multivariate methods.

微兆读数处存在污染。考虑到蒙特卡罗中使用的污染水平是实验获得的极限，我们可能仍然对这一贡献保持乐观。在第 4 节中，我们将展示如何利用电子扩散对我们的 TPC [13 记录的时间信号的影响，进一步减少读出平面附近的表面污染。最后，我们还必须认为我们的结果是保守的，因为通过增强现有的参数相关性，例如利用更复杂的多元方法，可能还有改进的余地。

We reserve any discussion on the discrimination potential of the topological parameters used in our analysis for section 3, where we will also argue on the benefit of introducing the twist parameter for our particular readout granularity, and we will assess the appropriateness of the two-dimensional 3 mm pitch detector choice as a baseline for the PandaX-III experiment.

我们保留在第 3 节的分析中使用的拓扑参数的辨别潜力的任何讨论，在这里我们还将讨论为我们的特定读出粒度引入扭曲参数的好处，并且我们将评估二维 3 毫米间距探测器选择作为 PandaX-III 实验基线的适当性。

11

3.Readout topology and granularity studies

3.读出拓扑和粒度研究

This section extends our study on background discrimination to different readout topologies and granularities.We will evaluate our new event reconstruction algorithms—detailed in appendix A—using two different readout layouts, a two-dimensional stripped layout and a three-dimensional pixel layout, to assess the potential gain on signal efficiency and/or background reduction.The results presented in this section will provide insight on the optimum readout scheme to be used in the PandaX-III data taking conditions, i.e. a vessel filled with 10 bar of xenon+TMA 1% gas mixture.We will discuss then the appropriateness of the PandaX-III baseline readout choice—detailed in appendix B.2—considering the advantages and disadvantages of two-dimensional versus three-dimensional event recon-struction, for different sizes of the readout channels, or detector granularity.

本节将我们对背景辨别的研究扩展到不同的读出拓扑和粒度。我们将使用两种不同的读出布局(二维剥离布局和三维像素布局)评估我们的新事件重建算法(详见附录 A)，以评估信号效率和/或背景降低的潜在增益。本节给出的结果将提供在 PandaX-III 数据采集条件下使用的最佳读出方案，即一个装有 10 巴氙+TMA 1%气体混合物的容器。然后，我们将讨论 PandaX-III 基线读出选择的适当性——详见附录 B . 2——考虑二维和三维事件重建的优缺点，对于不同尺寸的读出通道或探测器粒度。

We have re-processed the same datasets analyzed in section 2.However, this time we focus only on the U and Th background contributions originated in the vessel.The same processing chain -as described in appendix B.1—has been applied, being the readout used for event reconstruction the only modified element.We have systematically produced different readout structures in 2D and 3D at different pitch values.For the two-dimensional case, the 3 mm pitch PandaX-III baseline readout module design has been generalized to allow the definition of readout channels of any pitch

value.When defining a different pitch value we keep the size of the module unchanged, e.g. when we define a 1 mm pitch readout we increase the number of readout channels from 64 to 192.For the three-dimensional case we have simply designed a readout module using squared pixels, and for practical reasons we adapt the number of pixels to keep constant the size of the readout module as a function of the pixel size.We must remark anyhow that minor adjustments are required at the processing chain when dealing with different pitch sizes, e.g. the cluster distance used to identify tracks (see TRestHitsToTrackProcess description at appendix A.2) was set to 2.5× the pitch size, and the radius of the blob charge definition was fine tuned, being as low as R = 1 cm for 1 mm pitch, and as high as R = 2 cm for 1 cm pitch.

我们重新处理了第 2 节中分析的相同数据集。然而，这一次我们只关注起源于容器的铀和钍的背景贡献。已经应用了相同的处理链——如附录 B.1 所述——作为用于事件重建的读数，是唯一的修改元素。我们已经在 2D 和 3D 中以不同的间距值系统地产生了不同的读出结构。对于二维情况，3 毫米间距的 PandaX-III 基线读出模块设计已被推广到允许定义任何间距值的读出通道。当定义不同的间距值时，我们保持模块的大小不变，例如，当我们定义 1 mm 间距读出时，我们将读出通道的数量从 64 个增加到 192 个。对于三维情况，我们简单地设计了一个使用平方像素的读出模块，出于实际原因，我们调整了像素的数量，使读出模块的大小作为像素大小的函数保持不变。无论如何，我们必须注意，当处理不同间距尺寸时，在处理链上需要进行微小的调整，例如，用于识别轨迹的簇距离(参见附录 A.2 中的 TRestHitsToTrackProcess 描述)被设置为间距尺寸的 2.5 倍，并且斑点电荷定义的半径被微调，对于 1 毫米间距，低至 R = 1 厘米，对于 1 厘米间距，高至 R = 2 厘米。

In this particular study we seek to compare the rejection potential using different readout topologies.We must remark that the fiducialization response is not relevant for such goal, and we are interested to determine the topological rejection potential without those constraints.Therefore, an important difference with respect to the analysis of the previous section 2 is that we consider the full event interacting in the gas volume.In addition, our readout plane will fully cover the gas medium, or active area , so that the event reconstruction limits are just bound by the field cage wall defined in the Geant4 geometry.

在这项特殊的研究中，我们试图使用不同的读出拓扑来比较抑制电位。我们必须指出，基准化响应与此类目标无关，我们有兴趣确定没有这些约束的拓扑排斥势。因此，与前面第 2 节的分析相比，一个重要的区别是我们考虑了气体体积中的全部事件相互作用。此外，我们的读出平面将完全覆盖气体介质或活动区域，因此事件重建限制仅受 Geant4 几何图形中定义的场笼壁的限制。

Tables 3 and 4 show the effects of topological criteria, similar to those applied on section 2, for the simulated signal and background populations with different readout layouts and granularities.For each criterion (track energy ratio, blob charge and twist parameter) we provide the relative reduction, in percentage, with respect to the surviving event population from the previous criterion, or cut.We maximize our signal significance at each step by maximizing the quantity, s b .We observe that the reduction potential of the track energy ratio criterion is slightly better compared to the version where we included the fiducial detector response in section 2, i.e. by comparing the 3 mm pitch stripped readout results shown in table 3 with the values that can be deduced from table 1.This difference is mostly due to the fact that multi-track events have left the ROI after applying the detector response,

表 3 和表 4 显示了拓扑标准的效果，类似于第 2 节中应用的那些，针对具有不同读出布局和粒度的模拟信号和背景群体。对于每个标准(轨道能量比、斑点电荷和扭曲参数)，我们提供了相对于先前标准的幸存事件总数的相对减少(百分比)或切割。我们通过最大化数量来最大化每一步的信号重要性，⊠s·b· 。我们观察到，与我们在第 2 节中包括基准检测器响应的版本相比，轨道能量比标准的降低潜力略好，即通过将表 3 中所示的 3 mm 间距剥离读出结果与表 1 中可推导出的值进行比较。这种差异主要是由于在应用检测器响应后多轨道事件已经离开了投资回报，

Instead of using the 41-modules readout plane scheme described in appendix B.2, we extend the readout definition limits by adding readout modules as needed to cover the full active area.

我们没有使用附录 B.2 中描述的 41 模块读出平面方案，而是通过根据需要添加读出模块来扩展读出定义限制，以覆盖整个有效区域。

12

J.Phys. G: Nucl.Part.Phys. 47 (2020) 045108 J Galan et al

J.物理 G: Nucl。部分。《物理》47 (2020) 045108 J Galan 等人

Table 3.Relative signal efficiency and background reduction factors, in percentage, after each topological criterion, at different pitch values (1, 2, 3, 4 and 6 mm) for the two-dimensional stripped readout.The initial population of events considered at each step are the events in the ROI surviving from the previous criteria.Origin 1 mm 2 mm 3 mm

表 3 对于二维剥离读出，在不同的间距值(1、2、3、4 和 6 mm)下，每个拓扑标准后的相对信号效率和背景减少因子(百分比)。在每个步骤中考虑的初始事件群体是从先前标准中幸存下来的投资回报中的事件。原点 1 毫米 2 毫米 3 毫米

Isotope Xe U Th Xe U Th Xe U Th

同位素氙钍氙钍氙钍

Track Blob Twist

轨迹斑点扭曲

69.6 9.92 2.68 63.9 8.91 2.19 69.2 11.2 2.79

69.6 9.92 2.68 63.9 8.91 2.19 69.2 11.2 2.79

58.5 9.13 9.40 59.4 10.2 10.7 65.4 12.9 14.0

58.5 9.13 9.40 59.4 10.2 10.7 65.4 12.9 14.0

85.1 60.6 65.0 93.9 78.7 80.0 94.2 80.6 81.1

85.1 60.6 65.0 93.9 78.7 80.0 94.2 80.6 81.1

Total 34.6 0.55 0.16 35.6 0.71 0.19 42.6 1.16 0.32

总计 34.6 0.55 0.16 35.6 0.71 0.19 42.6 1.16 0.32

Origin 4 mm 6 mm

原点 4 毫米 6 毫米

Isotope Xe U Th Xe U Th

同位素氙钍氙钍

Track Blob Twist

轨迹斑点扭曲

73.1 13.2 3.33 79.2 16.7 4.37

73.1 13.2 3.33 79.2 16.7 4.37

64.2 14.1 14.5 54.2 12.3 12.2

64.2 14.1 14.5 54.2 12.3 12.2

94.0 83.2 81.6 90.2 82.5 74.4

94.0 83.2 81.6 90.2 82.5 74.4

Total 44.1 1.55 0.39 38.7 1.69 0.40

总计 44.1 1.55 0.39 38.7 1.69 0.40

Table 4.Relative signal efficiency and background reduction factors, in percentage, after each topological criterion, at different pitch values (2, 4, 6, 8 and 10 mm) for the three-dimensional pixel readout.The initial population of events considered at each step are the events in the ROI surviving from the previous criteria.Origin 2 mm 4 mm 6 mm

表 4 在三维像素读出的不同间距值(2、4、6、8 和 10 mm)下，每个拓扑标准后的相对信号效率和背景减少因子(百分比)。在每个步骤中考虑的初始事件群体是从先前标准中幸存下来的投资回报中的事件。原点 2 毫米 4 毫米 6 毫米

Isotope Xe U Th Xe U Th Xe U Th

同位素氙钍氙钍氙钍

Track Blob Twist

轨迹斑点扭曲

69.6 5.84 1.60 74.0 8.20 2.20 76.8 10.3 2.73

69.6 5.84 1.60 74.0 8.20 2.20 76.8 10.3 2.73

79.1 13.4 13.0 74.8 13.2 12.9 65.2 10.4 10.6

79.1 13.4 13.0 74.8 13.2 12.9 65.2 10.4 10.6

83.4 48.7 46.5 77.3 53.8 49.0 74.4 58.6 52.6

83.4 48.7 46.5 77.3 53.8 49.0 74.4 58.6 52.6

Total 45.9 0.38 0.097 42.8 0.58 0.14 37.3 0.63 0.15

总计 45.9 0.38 0.097 42.8 0.58 0.14 37.3 0.63 0.15

Origin 8 mm 10 mm

原点 8 毫米 10 毫米

Isotope Xe U Th Xe U Th

同位素氙钍氙钍

Track Blob Twist

轨迹斑点扭曲

78.8 12.0 3.3 80.3 13.6 3.75

78.8 12.0 3.3 80.3 13.6 3.75

68.0 10.6 10.7 64.1 10.8 9.72

68.0 10.6 10.7 64.1 10.8 9.72

——— ———

———————

Total 53.6 1.20 0.35 51.5 1.47 0.36

总计 53.6 1.20 0.35 51.5 1.47 0.36

and a subset of the background event population loses its multi-track features when we apply the detector response.

并且当我们应用检测器响应时，背景事件总体的子集失去了它的多轨道特征。

One interesting finding is that the newly introduced twist parameter starts to be efficient below 6 mm pitch, for both the two-dimensional and the three-dimensional readout versions.As observed in table 3, the 8 and 10 mm pitch pixel readouts studied did not improve the significance of the signal when using the twist parameter criterion.Figure 4 shows the evolution of the twist parameter and it confirms the advantage to differentiate signal and

一个有趣的发现是，对于二维和三维读出版本，新引入的扭转参数在 6 毫米间距以下开始有效。如表 3 所示，当使用扭转参数标准时，所研究的 8 和 10 mm 间距像素读数并没有提高信号的显著性。图 4 显示了扭曲参数的演变，证实了区分信号和

13

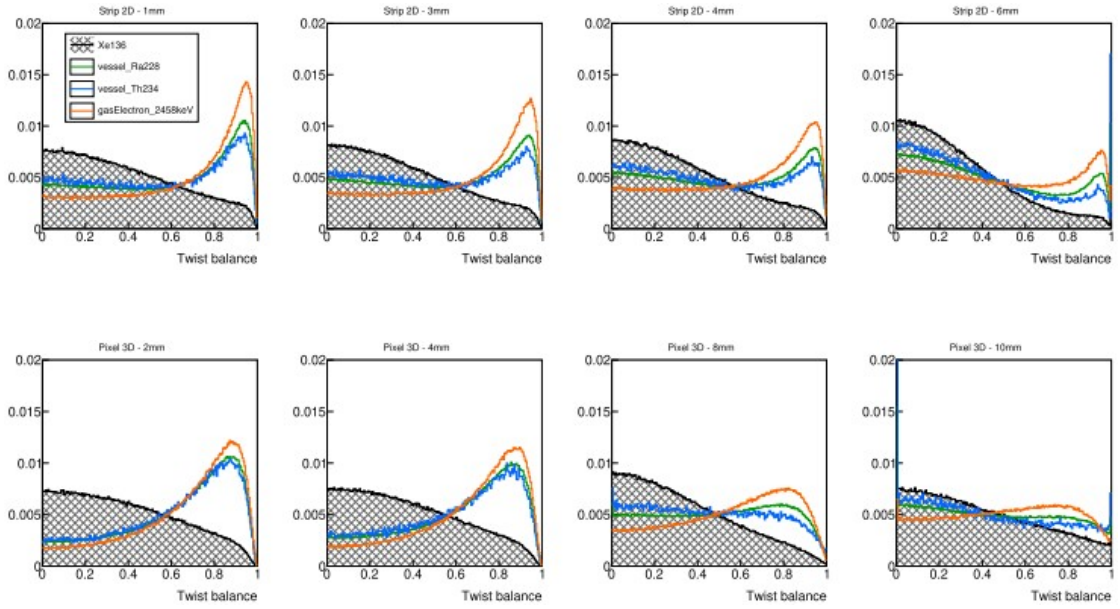

Figure 4.The distribution of the twist balance, ξb, parameter, a variant of the twist parameter calculated as x =- + ( )( ) x xx x b h lh l , being ξh the higher end-track twist parameter value, and ξl the lower end-track twist parameter value.The different plots show the evolution of this parameter for different detector granularities, and different readout topologies, 2D strips (top figures), and 3D pixels (bottom figures).The distribution from 0νββ signal events (filled curve) is compared to the background distribution of different contaminations as described in the text.For the 2D strips distributions only one of the projections is represented.

图 4 .捻度平衡参数 ξb 的分布，是捻度参数的一个变量，计算公式为 x =- + ( )( ) x xx x b h lh l，ξh 为较高的末端轨道捻度参数值，ξl 为较低的末端轨道捻度参数值。不同的图显示了不同检测器粒度、不同读出拓扑、2D 条纹(上图)和 3D 像素(下图)下该参数的演变。将 0νββ 信号事件的分布(填充曲线)与文本中描述的不同污染物的背景分布进行比较。对于 2D 条带分布，只显示了一个投影。

background distributions as the pitch value is reduced.Furthermore, we have added to this figure a third dataset where we generate single electrons with energy equal to the Qββ of Xe, demonstrating a small dependency on the quality of the topological observables related to the nature of the background source.

基音值减小时的背景分布。此外，我们在该图中添加了第三个数据集，其中我们生成了能量等于 Xe 的 Qββ 的单电子，证明了与背景源的性质相关的拓扑可观测性的质量的小的依赖性。

The twist parameter provides the less powerful topological criterion (as it is deduced from tables 3 and 4).However, we should take into account that this criterion operates after the event selection of track energy ratio and blob charge criteria.It is remarkable then that the twist parameter criterion is still capable to improve the signal significance, meaning that the twist parameter definition is an additional track feature that can be explored, exploited, and optimized in a future multivariate analysis that combines the track observables more efficiently.

扭曲参数提供了较弱的拓扑标准(从表 3 和表 4 中推导出来)。然而，我们应该考虑到，该标准在轨道能量比和斑点电荷标准的事件选择之后运行。值得注意的是，扭曲参数标准仍然能够提高信号显著性，这意味着扭曲参数定义是一个额外的轨迹特征，可以在未来的多变量分析中进行探索、开发和优化，从而更有效地组合轨迹观察值。

We summarize our results in figure 5, where we present the total signal significance, measured as s b , obtained with our topological criteria for different readouts.This figure allows us to assess now the gain on experimental sensitivity when reducing the detector granularity, and quantify the impact of using a two-dimensional readout compared to a three-dimensional one.We conclude from these results that the negative impact of using a stripped two-dimensional readout is counterbalanced by using a lower detector granularity, i.e. a 3 mm pitch two-dimensional readout is equivalent to a 1 cm pitch three-dimensional readout, with the advantage that the number of channels is reduced considerably in the two-dimensional version.

我们在图 5 中总结了我们的结果，其中我们给出了总信号显著性，以⊠s·b· 为例，用我们的拓扑标准获得了不同的读数。该图允许我们现在评估降低检测器粒度时实验灵敏度的增益，并量化使用二维读数与三维读数相比的影响。我们从这些结果中得出结论，使用剥离二维读出的负面影响通过使用较低的检测器粒度来抵消，即 3 mm 间距的二维读出相当于 1 cm 间距的三维读出，其优点是在二维版本中通道的数量显著减少。

14

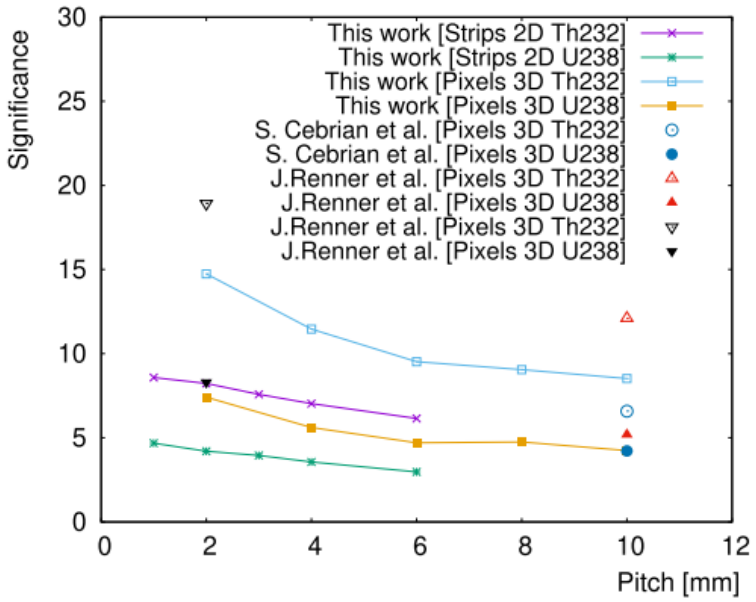

Figure 5.Total significance of topological criteria for the different detector granularities and topologies studied.The lines interconnecting data points show our results for the

图 5 .不同检测器粒度和拓扑结构的拓扑标准的总体重要性。连接数据点的线显示了我们的结果

two different contaminations studied (Th and U), and the two different readout topologies (Strips 2D and Pixels 3D).We add to this figure the significances obtained in previous studies, calculated from the background and signal efficiencies reported at

研究了两种不同的污染物(钍和铀)，以及两种不同的读出拓扑(条带 2D 和像素 3D)。我们将先前研究中获得的显著性加到这个数字上，这些显著性是根据以下报告的背景和信号效率计算出来的

[17, 19], and discussed in the text.

[17，19]，并在文中讨论过。

Moreover, we use figure 5 to compare our results to previously published studies—where they use similar conventional discrimination techniques.As it is observed, we find remark-ably good agreement with [17] on the final significance at 1cm 3D pixel readout, for both vessel contaminations.While, for [19], although we find reasonably compatible results for the U contamination chain (or Bi), we find their result on Th (or Tl) surprisingly high when compared to our data, being the origin of the main discrepancy at the level of the track energy ratio criterion.The difference between our results and those reported in [19] are even larger when we consider that their 1cm results correspond to pure xenon, and it was claimed in [17] that background reduction due to blob identification is worse by a factor 3 due to the higher electron diffusion in pure xenon, and that finally implies almost a factor 2 worse on significance.The source of this discrepancy might be related to the non-independent treatment of electron diffusion and detector granularity in [19], and the higher gas pressure, 15bar, of their setup.On the other hand, we should be cautious, since direct comparison of different setups is not always obvious.The significance of the criteria may depend not only on the origin, or the particular geometry of the setup, but also on the nature of the background and the target density, or detector pressure.We have seen, for example in figure 4, how a single electron track artificially launched from the gas volume, as it is done e.g. in [22], slightly generates better results in terms of the topological parameters quality.

此外，我们使用图 5 将我们的结果与之前发表的研究进行比较，这些研究使用了相似的传统鉴别技术。正如所观察到的，我们发现在 1cm 3D 像素读出的最终意义上，对于两种容器污染，与[17]非常好地一致。而对于[19]，尽管我们发现铀污染链(或铋)的结果相当一致，但我们发现它们在钍(或钋)上的结果与我们的数据相比高得惊人，这是在径迹能量比标准水平上主要差异的来源。当我们考虑到它们的 1cm 结果对应于纯氙时，我们的结果和[19]中报道的结果之间的差异甚至更大，并且在[17]中声称，由于斑点识别的背景减少差了 3 倍，这是由于纯氙中更高的电子扩散，并且这最终意味着显著性差了几乎 2 倍。这种差异的来源可能与[19 中电子扩散和探测器粒度的非独立处理以及它们设置的较高气压 15 巴有关。另一方面，我们应该谨慎，因为不同设置的直接比较并不总是显而易见的。标准的重要性可能不仅取决于原点或设置的特定几何形状，还取决于背景和目标密度或检测器压力的性质。我们已经看到，例如在图 4 中，单个电子轨道如何从气体体积人工发射，例如在[22 中所做的那样，在拓扑参数质量方面稍微产生更好的结果。

4.Fiducial background rejection in charge based TPC readouts

4.基于电荷的 TPC 读数中的基准背景抑制

The results obtained in section 2 unveiled the weakness of our topological cuts to discriminate surface contamination events originated from the Micromegas readout planes, as revealed by figure 3(a).Our setup lacks an absolute reference time, to, from the interactions taking place in

如图 3(a)所示，第 2 节中获得的结果揭示了我们的拓扑切割在区分源自微兆读出平面的表面污染事件方面的弱点。我们的设置缺少一个绝对的参考时间

15

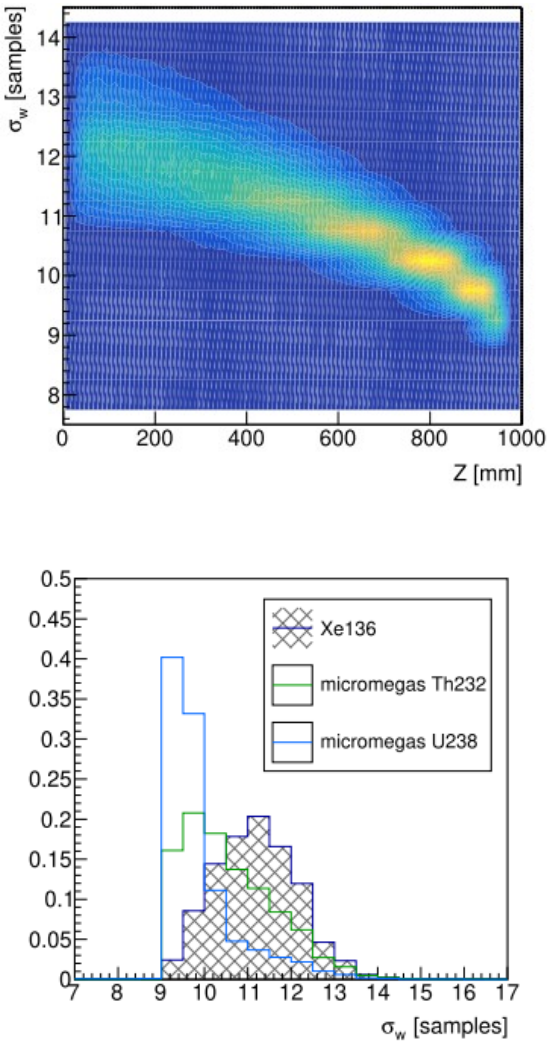

Figure 6.(a) A contour plot produced using the 0νββ signal event population, and showing the diffusion parameter, σw, as a function of the event position.Only one half of the symmetric TPC is shown here.Lower σw values correspond to events taking place near the readout plane, at z = 1000 mm, and larger values correspond to events taking place near the cathode, at z = 0 mm. (b) The distribution of the σw parameter for 0νββ signal events (filled curve), and the two background Micromegas components studied.

图 6 .使用 0νββ 信号事件总体产生的等值线图，显示扩散参数 σw，作为事件位置的函数。此处仅显示了对称 TPC 的一半。较低的 σw 值对应于在 z = 1000 mm 时发生在读出平面附近的事件，较大的值对应于在 z = 0 mm 时发生在阴极附近的事件。(b)0νββ 信号事件的 σw 参数分布(填充曲线)，以及所研究的两个背景微兆分量。

the detector volume.Without such a reference we cannot directly determine the event absolute z-position, making it hard to discriminate surface events originated on the readout planes, or the cathode.

探测器体积。如果没有这样的参考，我们就不能直接确定事件的绝对 z 位置，这使得很难区分表面事件起源于读出平面或阴极。

In this section we develop a basic technique to demonstrate the remaining potential for further background reduction by attenuating the negative impact of surface contamination, even in the absence of to.For that we take advantage of the readout signal dependence on the diffusion of

ionized electrons drifting towards the readout planes.The time signals induced on the Micromegas readout, due to a particular energy deposition on the TPC volume, will be broader when the electron cloud has drifted a longer distance towards the readout plane.However, the resulting primary electrons from β-tracks generated near the readout plane will drift a very short distance, and therefore the original charge distribution will be almost unaffected by the electron drift.

在这一节中，我们开发了一种基本技术，通过减弱表面污染的负面影响来展示进一步降低背景的剩余潜力，即使在没有 to 的情况下也是如此。为此，我们利用了读出信号依赖于向读出平面漂移的电离电子的扩散。当电子云向读出平面漂移更长的距离时，由于热等离子体体积上的特定能量沉积，在微兆读出上感应的时间信号将更宽。然而，从读出平面附近产生的 β 轨道得到的初级电子将漂移非常短的距离，因此原始电荷分布将几乎不受电子漂移的影响。

We have re-processed the 0νββ signal and Micromegas background datasets analyzed in previous sections using the same data chain parameters as defined in section 2.However, now we need to include few additional effects in order to extract a parameter, σw, that correlates to the diffusion of electrons in the gas.The generation of this parameter is performed under realistic conditions including the signal shaping introduced by electronics and a typical electronic noise level (further details on the extraction of this parameter are given in appendix C).In figure 6 we observe the desired dependence of σw with the z-position of the simulated 0νββ event, together with the σw distribution produced by the two Micromegas background components compared to the 0νββ signal one.We observe clearly how back-ground surface events peak at low values of σw.

我们使用第 2 节中定义的相同数据链参数，重新处理了前几节中分析的 0νββ 信号和 Micromegas 背景数据集。然而，现在我们需要包括一些额外的影响，以便提取一个参数，σw，它与电子在气体中的扩散有关。该参数的产生是在现实条件下进行的，包括由电子器件引入的信号整形和典型的电子噪声水平(该参数提取的进一步细节在附录 C 中给出)。在图 6 中，我们观察到 σw 与模拟的 0νββ 事件的 z 位置的期望相关性，以及两个 Micromegas 背景分量产生的 σw 分布与 0νββ 信号分量的比较。我们清楚地观察到背景地表事件如何在 σw 的低值处达到峰值。

Therefore, we exploit the properties of σw to introduce an additional selection criterion in our data by accepting only the population of events that are above a certain diffusion threshold, as quantified by σw. Table 5 presents the results on event acceptance after applying

因此，我们利用 σw 的特性，通过仅接受超过某个扩散阈值的事件总体，在我们的数据中引入一个额外的选择标准，如 σw 所量化的。表 5 给出了应用后事件接受的结果

16

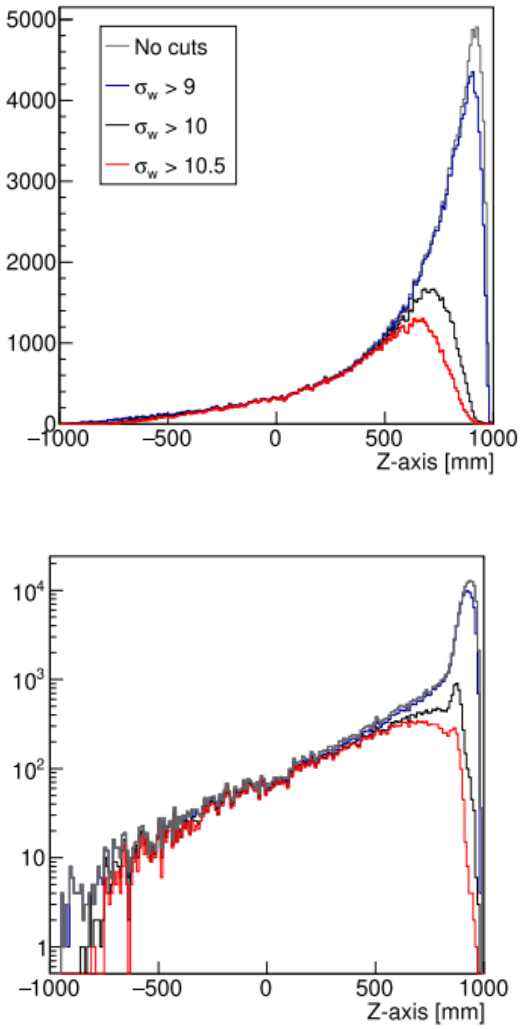

Figure 7.Distribution of the average z-position for events produced by Th (a), in

图 7 .Th (a)产生的事件的平均 z 位置分布，单位为

linear scale, and U (b), in logarithmic scale, generated from the Micromegas readout plane, placed at z = 1000 mm. Different curves represent the background reduction after applying different threshold values on the diffusion parameter, σw. The initial population of events, tagged as 'No cuts', are the events found in our ROI definition.

线性标度和对数标度的 U (b)，由放置在 z = 1000 毫米的微兆读出平面产生。不同的曲线表示在扩散参数 σw 上应用不同阈值后的背景减少。标记为“无切割”的初始事件群体是在我们的投资回报定义中发现的事件。

Table 5.Overall background reduction, in percentage, for events generated from the

表 5 事件生成的总背景减少百分比

Micromegas readout plane, Th and U contaminations, and the corresponding signal efficiency, after applying different cuts on the diffusion parameter, σw.

在扩散参数 σw 上施加不同的切割之后，微兆读出平面、钍和铀污染以及相应的信号效率

σw > 9 σw > 10 σw > 10.5

σw > 9 σw > 10 σw > 10.5

Th 93.3 53.7 44.4 U 80.9 20.1 15.1 136Xe 99.4 83.0 74.5

th 93.3 53.7 44.4 U 80.9 20.1 15.1 136 XE 99.4 83.0 74.5

cuts for different threshold values, where we observe that we manage to reduce by an additional factor 0.15 the contribution from the U chain, due to Bi decays, while keeping our signal efficiency near 75%.We must remember that the Micromegas contribution of U was a dominant component in table 2.The background reduction on the U chain is more significant than in the Th chain, due to the fact that the 2614 keV gamma from Tl is produced in almost any decay, generating finally a higher ratio of volume to surface events compared to the Bi contribution, which produces a β decay with high energy gamma emission only at 1.5% of the decays.We should remark that the values presented on table 5 have been obtained without applying topological cuts.Still, these results are independent on previous topological cuts, since we do not observe any dependence on the z-distribution after cuts, as it would have been revealed by the 0νββ population in figure 3(b), after the topo-logical analysis performed in section 2.

不同阈值的切割，我们观察到，由于 Bi 衰减，我们设法将 U 链的贡献降低了 0.15 倍，同时保持信号效率接近 75%。我们必须记住，在表 2 中，铀的微兆贡献是一个主要成分。U 链上的背景减少比 Th 链上的更显著，这是因为来自 Tl 的 2614 keV 几乎在任何衰变中产生，最终产生比 Bi 贡献更高的体积与表面事件比率，这产生 β 衰变，仅在衰变的 1.5%产生高能 γ 发射。我们应该注意，表 5 中给出的值是在不应用拓扑切割的情况下获得的。尽管如此，这些结果独立于以前的拓扑切割，因为我们没有观察到切割后 z 分布的任何依赖性，正如在第 2 节进行拓扑分析后，图 3(b)中的 0νββ 总体所揭示的那样。

Finally, in figure 7 we show the background distribution as a function of the event position, for each of the two Micromegas isotope contaminations, after applying different sw threshold values.In these figures we observe how all the events from surface nature have been completely removed already for σw > 10, and how the remaining background event

最后，在图 7 中，我们显示了在应用不同的 sw 阈值后，两种微兆同位素污染的背景分布作为事件位置的函数。在这些图中，我们观察到，对于 σw > 10，表面性质的所有事件是如何被完全去除的，以及剩余的背景事件是如何被完全去除的

17

J.物理 G: Nucl。部分。《物理》47 (2020) 045108 J Galan 等人

population on table 5, i.e. 20.1% for U and 53.7% for Th, are only due to volume events that can only be removed by exploiting topological event features.

表 5 中的人口，即 20.1%的铀和 53.7%的钍，仅仅是由于体积事件，只能通过利用拓扑事件特征来消除。

5.Conclusions

5.结论

In this work, we have presented results on topological background discrimination considering a realistic detector response for the PandaX-III TPC baseline design.The realistic response includes an accurate description of the existing Micromegas detector layout used for the reconstruction of events in a similar way as it is done with experimental data.However, the most important element on the detector response relies on an appropriate definition of the energy of each event by considering the electronic acquisition window and the readout plane boundaries of the PandaX-III design.

在这项工作中，我们已经提出了拓扑背景鉴别的结果，考虑了一个现实的探测器对潘达克斯-三型热等离子体发生器基线设计的响应。真实的反应包括对现有微兆探测器布局的准确描述，该布局用于以与实验数据相似的方式重建事件。然而，探测器响应的最重要因素依赖于对每个事件能量的适当定义，通过考虑电子采集窗口和 PandaX-III 设计的读出平面边界。

We observe a negative effect on our topological background discrimination when we apply the detector response to the Monte Carlo event data, hence the importance to include those effects in our study.The results obtained show that a promising final background level is achievable.Using topological arguments, we find that for a signal reduction of ∼1/3 we can achieve a reduction factor of about 100 on the background contamination.Even after including the detailed detector response, this result is still in good agreement with the pre-liminary estimate used to calculate the sensitivity of the first PandaX-III module at [9].

当我们将探测器响应应用于蒙特卡罗事件数据时，我们观察到拓扑背景辨别的负面影响，因此在我们的研究中包括这些影响非常重要。获得的结果表明，有希望的最终背景水平是可以实现的。使用拓扑参数，我们发现对于∨1/3 的信号减少，我们可以在背景污染上实现大约 100 的减少因子。即使包括了详细的探测器响应，这个结果仍然与用于计算[9 号的第一个 PandaX-III 模块的灵敏度的初步估计一致。

It is remarkable that the overall background contribution of the detector vessel will be negligible for the lifetime of the experiment.While an acceptable value for the contribution of one of the most uncertain sources of background in the experiment—the detector readout plane—results in a conservative contribution of 12 counts per year.

值得注意的是，在整个实验过程中，探测器容器的总背景贡献可以忽略不计。虽然实验中最不确定的背景源之一——探测器读出平面——的贡献的可接受值导致每年 12 个计数的保守贡献。

Furthermore, we demonstrate the capability of our setup to perform a fiducialization in the z-axis even in the absence of to, and remove a considerable amount of surface background events that cannot be eliminated by other means.By exploiting this technique we are able to reduce the Micromegas background contribution to levels well below 1 count per year, preserving 80% of the $0\nu\beta\beta$ signal.

此外，我们还展示了我们的装置即使在没有 to 的情况下也能在 z 轴上进行基准化，并消除大量无法用其他方法消除的表面背景事件的能力。通过利用这一技术，我们能够将微兆的背景贡献降低到远低于每年 1 个计数的水平，保留 80%的 $0\nu\beta\beta$ 信号。

We have also addressed the question relative to the impact of a two-dimensional readout on the pattern recognition of $0\nu\beta\beta$.It is obvious that the lack of a full three-dimensional event reconstruction leads to a reduced discrimination power.In the two-dimensional case, our event identification and classification must be based on two projections of the event, and necessarily some of those event projections hide information that can only be revealed by a three-dimensional reconstruction.Occasionally, a secondary track will be hidden by the projection and counted as energy of the main track, affecting the track energy ratio criterion, while in other events, the integration of the charge of an electron moving orthogonally to the projection may mimic a blob, reducing the rejection power of the blob charge and the twist parameter criteria.We have

systematically studied the significance of our topological criteria for different detector granularities at three-dimensional pixel and two-dimensional stripped readout designs, concluding that the negative impact on two-dimensional readout pattern recognition is counterbalanced by a reduced detector granularity, i.e. a 1 cm pixel readout reaches an event topological rejection power comparable to a 3 mm stripped readout.Con-sequently, the 3 mm pitch stripped baseline readout choice for PandaX-III detector is much more convenient, not only in terms of detector design complexity due to the reduced number of channels required, but also minimizing the impact of typically non-radiopure electronics equipment near the detector readout planes.

我们还解决了二维读数对 0νββ 模式识别的影响问题。很明显，缺乏完整的三维事件重建导致辨别能力降低。在二维情况下，我们的事件识别和分类必须基于事件的两个投影，并且这些事件投影中的一些必然隐藏了只能通过三维重建揭示的信息。偶尔，次轨道将被投影隐藏，并被计为主轨道的能量，从而影响轨道能量比标准，而在其他情况下，垂直于投影移动的电子的电荷的积分可能模拟斑点，降低斑点电荷的抑制能力和扭曲参数标准。我们系统地研究了我们的拓扑标准对于三维像素和二维剥离读出设计的不同检测器粒度的重要性，结论是对二维读出模式识别的负面影响被降低的检测器粒度所抵消，即 1 cm 像素读出达到与 3 mm 剥离读出相当的事件拓扑抑制能力。因此，对于 PandaX-III 探测器，3 毫米间距剥离基线读出选择更加方便，不仅因为所需通道数量减少，探测器设计更加复杂，而且还最大限度地减少了探测器读出平面附近典型的非辐射电子设备的影响。

We have introduced novel track parameters, as the end-track twist and the track length, never exploited before on the pattern recognition of 0νββ using conventional techniques.We

我们引入了新的轨迹参数，如末端轨迹扭曲和轨迹长度，这在使用传统技术的 0νββ 模式识别中是前所未有的。我们

18

have assessed their discrimination potential, and observed how the end-track twist feature is still contributing to the signal-to-background significance, even after filtering the event population previously with other topological criteria, as the track energy ratio and the blob charge.Furthermore, we have found that this parameter is relevant for pattern recognition when the detector granularity is below 6 mm, concluding that such granularity or better is necessary to reveal the aforementioned track features.

已经评估了它们的辨别能力，并观察到即使在使用其他拓扑标准(如轨迹能量比和斑点电荷)过滤事件总体后，末端轨迹扭曲特征仍对信号背景显著性有贡献。此外，我们发现当检测器粒度低于 6 mm 时，该参数与模式识别相关，从而得出这样的粒度或更好的粒度对于揭示上述轨迹特征是必要的结论。

We believe our results are conservative, and that there exists room for improvement and optimization through multivariate methods that better exploit the different parameter correlations.Additionally, exploring the use of novel track parameters, or improving the existing ones, can push the conventional background discrimination further.Additional parameters, as the dE/dx along the track, previously studied at [23], and its peculiarities at the end-tracks could allow to improve these results by properly combining them with the parameters studied in this work.

我们相信我们的结果是保守的，并且通过更好地利用不同参数相关性的多变量方法存在改进和优化的空间。此外，探索使用新的轨迹参数，或者改进现有的轨迹参数，可以进一步推动传统的背景辨别。额外的参数，如沿轨道的 dE/dx，以前在[23]研究过，以及其在末端轨道的特性，可以通过将它们与本工作中研究的参数适当结合来改善这些结果。

Recently, we have seen how machine learning methods provide enhanced capabilities for pattern recognition, as reported in [19, 22, 24].These techniques, which provide excellent signal-to-background discrimination ratios, could never replace a conventional analysis.In a conventional analysis the different topological parameters serve as a mechanism to control the goodness of the Monte Carlo event reconstruction.In other words, we will be able to validate the different event parameters obtained by comparing with the experimental data, allowing us to be confident on our event reconstruction and the effectiveness of our topological criteria.The use of machine learning techniques, without further or complementary analysis, will not be sufficient by itself to prove the background of the detector.

最近，我们已经看到机器学习方法如何为模式识别提供增强的能力，如[19，22，24 所报道的。这些技术提供了极好的信号与背景鉴别率，永远无法取代传统的分析。在常规分析中，不同的拓扑参数用作控制蒙特卡罗事件重构的良好性的机制。换句话说，我们将能够验证通过与实验数据比较而获得的不同事件参数，从而使我们对我们的事件重建和我们的拓扑标准的有效性有信心。如果没有进一步的或补充的分析，机器学习技术的使用本身不足以证明检测器的背景。

The present work served to demonstrate the existing software infrastructure implemented in REST for event reconstruction, and the flexibility to add a detailed detector response at different levels, as necessary.REST has been conceived to provide a high degree of mod-ularity allowing to connect or disconnect different event processes at any place of the event data processing chain.We have designed dedicated event processes and metadata structures to construct the PandaX-III Monte Carlo processing chain.Still, additional details can be included in future studies, that may implement even more realistic event reconstruction.A future Monte Carlo event processing may consider further details ignored in this work, as e.g. the gap inter-distance between neighbor readout modules, or the necessary deconvolution of the electronic signal shaping.

当前的工作用于演示在 REST 中实现的用于事件重建的现有软件基础设施，以及根据需要在不同级别添加详细检测器响应的灵活性。REST 旨在提供高度的模块化，允许在事件数据处理链的任何位置连接或断开不同的事件进程。我们已经设计了专用的事件流程和元数据结构来构建 PandaX-III 蒙特卡罗处理链。尽管如此，更多的细节可以包括在未来的研究中，这可能实现更现实的事件重建。未来的蒙特卡罗事件处理可以考虑在本工作中忽略的更多细节，例如相邻读出模块之间的间隙间距，或者电子信号整形的必要去卷积。

Finally, when comparing to real experimental conditions we will need to consider dif-ferent systematic effects due to different parameters that may fluctuate, or change, during the data taking periods of the experiment, such as the electronic noise, the drift field intensity or irregularities, the concentration of TMA and its effect on the gas properties, the gain inho-mogeneities on each detector module, the effect of readout module gaps on the event reconstruction, possible dead channels in the detectors, etc.All those studies must be addressed in the near future in order to have full control on the detector performance.The present work represents a necessary step towards those studies.

最后，当与实际实验条件进行比较时，我们需要考虑不同的系统效应，这些效应是由于在实验的数据采集期间可能波动或变化的不同参数造成的，例如电子噪声、漂移场强度或不规则性、TMA 的浓度及其对气体特性的影响、每个探测器模块上的增益不均匀性、读出模块间隙对事件重建的影响、探测器中可能的死通道等。所有这些研究必须在不久的将来进行，以便完全控制探测器的性能。目前的工作代表着向这些研究迈出的必要一步。

Acknowledgments

感谢

B Jiang and S Wu acknowledge support from The Zhiyuan Scholar Program (Grants No. ZIRC2016-01 and No. ZIRC2017-05).J Galan acknowledges support from the Chung-Yao Chao fellowship program.

蒋和吴树声对致远奖学金项目(资助号:2016-01 和 2017-05)的支持表示感谢。加兰感谢赵忠尧奖学金计划的支持。

Appendix A. REST as a data analysis framework

附录 A .作为数据分析框架的可再生能源技术

Rare Event Searches with TPCs Software (RESTSoft) is a collaborative software effort providing a common framework for acquisition, simulation, and data analysis for gaseous TPCs [25].REST is composed of a set of libraries written in C++ and is fully integrated in ROOT [26], i.e. all REST classes inherit from TObject and can be read/accessed/written using the ROOT I/O interface.The only structural dependence is related to ROOT libraries, while other packages, as Geant4 [27] or Garfield++ [28], can be optionally integrated and used within the REST framework when generating or processing Monte Carlo data.

罕见事件搜索与热动力传输控制系统软件(RESTSoft)是一个合作软件的努力，提供了一个通用的框架，为气体热动力传输控制系统的采集，模拟，和数据分析[25]。REST 由一组用 C++编写的库组成，并且完全集成在根[26]中，即所有 REST 类都继承自对象，并且可以使用根 I/O 接口进行读取/访问/写入。唯一的结构依赖与 ROOT 库有关，而其他包，如 Geant4 [27]或 Garfield++ [28]，在生成或处理蒙特卡洛数据时，可以在 REST 框架内进行集成和使用。

During the last years, major upgrades took place on the REST core libraries [29].An important feature introduced in REST is that metadata and event data are stored together in a unique file.We understand by metadata any information required to give meaning to the data registered in the event data, as it can be the initial run data taking conditions, the geometry of the detector, the gas properties, or the detector readout topology.Additionally, any input or output parameters, required during the processing or transformation of event data, using event processes, will be stored as metadata.Any previous existing metadata structures inside the REST input file will be transferred to any future output, assuring full traceability, as well as reproducibility of results obtained with a particular dataset.

在过去的几年里，主要的升级发生在[29]的 REST 核心图书馆。REST 引入的一个重要特性是元数据和事件数据一起存储在一个唯一的文件中。我们通过元数据了解赋予事件数据中记录的数据以意义所需的任何信息，因为它可以是初始运行数据获取条件、探测器的几何形状、气体属性或探测器读出拓扑。此外，使用事件进程处理或转换事件数据期间所需的任何输入或输出参数都将存储为元数据。REST 输入

文件中任何先前存在的元数据结构都将被转移到任何未来的输出中，以确保完全的可追溯性，以及用特定数据集获得的结果的可再现性。

An ambitious feature of REST is its capability to analyze Monte Carlo and experimental data using common event processes.This is possible by using existing REST event processes to condition the input data generated, for example, by a Geant4 Monte Carlo simulation.After an appropriate event data conditioning, our Monte Carlo generated event will reproduce the rawdata of the detector (as it is shown in appendix C).Once we are at that stage, we can benefit from using the same event processes to analyze Monte Carlo and real experimental data.A realistic Monte Carlo rawdata reconstruction will allow us to assess, validate and optimize the processes that will be involved in the real event reconstruction and analysis even before the start of the physics run of the experiment.

REST 的一个雄心勃勃的特点是它能够使用普通事件过程分析蒙特卡罗和实验数据。这可以通过使用现有的 REST 事件过程来调节输入数据，例如，通过 Geant4 蒙特卡罗模拟。经过适当的事件数据处理后，我们的蒙特卡罗生成事件将再现探测器的原始数据(如附录 C 所示)。一旦我们到了那个阶段，我们就可以从使用相同的事件过程来分析蒙特卡罗和真实的实验数据中获益。一个现实的蒙特卡罗原始数据重建将使我们能够评估、验证和优化将涉及真实事件重建和分析的过程，甚至在实验的物理运行开始之前。

In the following subsections, we recall the definitions of the different components of REST, viz event types, event processes, and analysis tree.These definitions will serve as a reference for the article.Note that we do this having in mind the case where the physics variables of interest are local energy deposits, called hits, and the signal is digitized by a sampling ADC The REST software is versatile enough, though, to handle many other cases.We include here only those components of REST that are relevant to our study.

在下面的小节中，我们回顾了 REST 的不同组件的定义，即事件类型、事件过程和分析树。这些定义将作为本文的参考。请注意，我们这样做是考虑到感兴趣的物理变量是局部能量沉积(称为 hits)的情况，信号由采样模数转换器(ADC)数字化。不过，rest 软件功能强大，足以处理许多其他情况。这里我们只包括与我们的研究相关的 REST 的那些组成部分。

A.1. Event types

答:1 .事件类型

REST defines basic event types, or data structures, commonly used to store event data generated during the data acquisition (DAQ), production and/or event data processing.The definition of a reduced set of basic event types allows for better inter-process connectivity.The following data structures defined in REST are used in our study.

REST 定义了基本的事件类型或数据结构，通常用于存储在数据采集(DAQ)、生产和/或事件数据处理过程中生成的事件数据。简化的基本事件类型集的定义允许更好的进程间连接。在我们的研究中使用了 REST 中定义的以下数据结构。

• TRestHitsEvent: This structure contains an arbitrary number of elements or hits used to store a physical variable, fi, defined in a three-dimensional coordinate system (xi, yi, zi).In our study, we use this event type to describe the energy depositions on the volume of the detector.

三进制:该结构包含任意数量的元素或命中，用于存储在三维坐标系中定义的物理变量 fi(Xi、易、子)。在我们的研究中，我们使用这种事件类型来描述探测器体积上的能量沉积。

• TRestG4Event: It is a natural extension of TRestHitsEvent containing additional information gathered during the Geant4 simulation, such as the physical interaction associated to the hit, and the volume of the simulation geometry where the interaction took place.

TRESTg4 事件:它是 TRestHitsEvent 的自然延伸，包含在 Geant4 模拟过程中收集的附加信息，例如与命中相关的物理交互，以及发生交互的模拟几何体的体积。

20

• TRestTrackEvent: A more sophisticated structure where hits are grouped into tracks, following e.g. a proximity criterion.Tracks can, in turn, be grouped into higher level structures.An identification number and a parent number are assigned to each object and allow to keep the record of its genealogy.A track that is not associated to a parent track will be denominated as an origin track, while a track with no daughter tracks will be denominated as a top-level track.Therefore, in this scheme we may distinguish different track levels related to the number of track generations.

TRestTrackEvent:一种更复杂的结构，其中点击被分组到轨道中，遵循例如接近标准。反过来，轨道可以被分组到更高层的结构中。每个对象都有一个标识号和一个父编号，并允许保留其谱系记录。不与父轨道相关联的轨道将被命名为原始轨道，而没有子轨道的轨道将被命名为顶级轨道。因此，在该方案中，我们可以区分与轨道世代数相关的不同轨道等级。

• TRestRawSignalEvent: Stores the digitized signal samples, in the shape of fixed size arrays.Each array corresponds to one front-end electronics channel, and is assigned a logical signalId.The set of signalId’s is mapped to the geometry of the detection with help of a readout metadata table, typically known as decoding.The arrays generally describe the time evolution of the signal.

TRestRawSignalEvent:以固定大小阵列的形式存储数字化信号样本。每个阵列对应一个前端电子通道，并分配一个逻辑信号。借助于读出的元数据表，这组信号被映射到检测的几何图形，通常称为解码。阵列通常描述信号的时间演变。

• TRestTimeSignalEvent: It contains an arbitrary number of non-fixed size arrays that define a physical quantity, fi , at arbitrary times, ti, expressed in physical time units.Each array dataset may contain a different number of data points.This kind of event type can be exploited, e.g. for experimental data reduction or storage of timed signals produced in Monte Carlo generated data.As in the case of a TRestRawSignalEvent, each array is also identified using a signalId associated to the electronic channels described inside the readout metadata description.

TRestTimeSignalEvent:它包含任意数量的非固定大小的数组，这些数组定义了任意时间的物理量 fi，ti，以物理时间单位表示。每个数组数据集可以包含不同数量的数据点。这种类型的事件可以被利用，例如用于实验数据的减少或在蒙特卡洛生成的数据中产生的定时信号的存储。与 TRestRawSignalEvent 的情况一样，每个阵列也使用与读出元数据描述中描述的电子通道相关联的信号标识来识别。

We stress again that the event types defined in REST aspire to be as generic and abstract as possible.It is the role of processes, and other metadata information used during the data processing, to provide a physical meaning, or final interpretation, to the information that is contained in our event type.In the scenario where certain specialization is required, as it is the case of a

TRestG4Event, an existing REST event process will be capable to transform this specialized, or dedicated, event type into an existing and more basic one, as it is a TRestHitsEvent.

我们再次强调，REST 中定义的事件类型希望尽可能通用和抽象。它是流程的角色，以及在数据处理过程中使用的其他元数据信息，为我们的事件类型中包含的信息提供物理意义或最终解释。在需要特定专门化的场景中，如 REST 事件的情况，现有的 REST 事件流程将能够将这种专门化的或专用的事件类型转换为现有的更基本的事件类型，因为它是 TRestHitsEvent。

The event types described are not only containers to store event data in REST, but they implement methods associated to the nature of each data structure, as e.g. spatial rotation or translation of coordinates in a TRestHitsEvent or time signal processing methods in a TRestRawSignalEvent, as e.g. differentiation, smoothing or Fast Fourier Transform (FFT) methods, together with prototyped methods, i.e. common to all the event types, for visualizing and printing the contents of a particular stored event.

所描述的事件类型不仅是在 REST 中存储事件数据的容器，而且它们实现了与每个数据结构的性质相关联的方法，例如在 TRestHitsEvent 中的坐标的空间旋转或平移，或者在 TRestHitsEvent 中的时间信号处理方法，例如微分、平滑或快速傅立叶变换(FFT)方法，以及原型方法，即所有事件类型所共有的方法，用于可视化和打印特定存储事件的内容。

A.2. Event processes

事件流程

REST offers a large variety of event processes operating on the basic event types in order to manipulate the event data, transform it and extract relevant information in the intermediate steps taking place during a particular event data processing chain.An event process in REST is modular, and it can be integrated in REST by fixing only its input and output event types.In other words, any event process that participates in a data processing chain must satisfy that its input event type corresponds with the output event type of the previous event process, although there are exceptions as will be described in appendix A.3.

REST 提供了对基本事件类型进行操作的各种各样的事件过程，以便在特定事件数据处理链期间发生的中间步骤中操纵事件数据、对其进行转换并提取相关信息。REST 中的事件进程是模块化的，它可以通过只修复其输入和输出事件类型而集成到 REST 中。换句话说，任何参与数据处理链的事件过程都必须满足其输入事件类型与前一个事件过程的输出事件类型一致，尽管如附录 A.3 所述存在例外

Therefore, event processes can be classified as processes that transform an event type into another, i.e. conversion processes, and those which operate in a particular event type, i.e. hit, raw signal or track processes, in which the output event type remains unchanged (although its content—the event data—will usually be transformed).In the following sub-sections we provide a description of the different processes involved in our data processing.A full,

因此，事件过程可以被分类为将事件类型转换为另一种类型的过程，即转换过程，以及在特定事件类型中操作的过程，即命中、原始信号或跟踪过程，其中输出事件类型保持不变(尽管其内容——事件数据——通常将被转换)。在下面的小节中，我们将描述数据处理中涉及的不同过程。一个完整的，

detailed and up-to-date list of documented processes will be available at the REST API Documentationfor further reference.

详细的和最新的文件化过程列表将在 REST 应用编程接口文件中提供，以供进一步参考。

A.2.1. Conversion processes.

A.2.1 .转换过程。

• TRestG4ToHitsProcess: A simple process to transform a TRestG4Event into a TRestHitsEvent, visualized in figure A1(a).Any specific hits information related to Geant4 will be lost after this step.Then, the only way in REST to have this information available at the end of the data processing chain will be through the analysis tree, described in appendix A.3.

TRestG4ToHitsProcess:将 trestg 4 事件转换为 TRestHitsEvent 的简单过程，如图 A1(a)所示。在此步骤之后，任何与 Geant4 相关的特定点击信息都将丢失。然后，在 REST 中，在数据处理链的末端获得这些信息的唯一方法是通过分析树，如附录 A.3 所述

• TRestHitsToSignalProcess: This process produces a time projection of the primary electron positions in the TPC volume into the readout plane of the detector, producing the result shown in figure A1(c).The coordinates of hits (xi, yi, zi) stored in a TRestHitsEvent are transformed into a TRestTimeSignalEvent.This process uses the REST readout metadata structure (described in detail in appendix B.2) to associate each hit coordinates (xi, yi) with a detector readout channel, and perform a spatial to time conversion of the zi coordinate using the readout plane position and the drift velocity of electrons in the gas.The gas properties can be introduced directly as an input metadata parameter, or extracted from a specific metadata class, named TRestGas, that interfaces with Garfield++ to obtain the properties of any gas mixture as calculated by Magboltz.A sampling time, δ t, can be provided optionally to discretize the resulting time values at the output TRestTimeSignalEvent.

TRestHitsToSignalProcess:该过程产生 TPC 体积中初级电子位置到探测器读出平面的时间投影，产生如图 A1(c)所示的结果。存储在一个三叉树中的命中坐标(xi，易，子)被转换成一个三叉树信号事件。该过程使用 REST 读出元数据结构(在附录 B.2 中详细描述)将每个命中坐标(xi，yi)与检测器读出通道相关联，并使用读出平面位置和气体中电子的漂移速度执行 zi 坐标的时空转换。气体属性可以作为输入元数据参数直接引入，或者从名为 TRestGas 的特定元数据类中提取，该类与 Garfield++接口，以获得由 Magboltz 计算的任何气体混合物的属性。可以选择提供采样时间 δ t，以离散输出端的结果时间值。

• TRestSignalToHitsProcess: The inverse process of a TRestHitsToSignalProcess, produ-cing the result shown in figure A1(d).We recover, or reconstruct, the hit coordinates using the time information inside a TRestTimeSignalEvent and the gas properties.The reconstructed coordinates are obtained using the readout metadata description and the corresponding readout channel number, associated to each signalId.

tretsiginaltohitprocess:tretsitstosignalprocess 的逆过程，产生如图 A1(d)所示的结果。我们使用一个 TRestTimeSignalEvent 中的时间信息和气体属性来恢复或重建击中坐标。使用读出元数据描述和对应的读出通道号获得重建的坐标，与每个信号指示相关联。

• TRestSignalToRawSignalProcess: This process takes as input a TRestTimeSignalEvent type and samples its contents into a fixed data array compatible with the TRestRawSignalEvent output type, i.e. fixing the number of data points and sampling time, δt, which are provided as an input

parameter to this process.A reference time, or trigger definition, is used to define the physical time corresponding to the first sample of the resulting data array.Figure A2 describes one of the trigger methods available on this process which we use later in this study.

TRestSignalToRawSignalProcess:该过程将 TRestTimeSignalEvent 类型作为输入，并将其内容采样到与 TRestRawSignalEvent 输出类型兼容的固定数据数组中，即固定数据点数和采样时间 δt，它们作为输入参数提供给该过程。参考时间或触发器定义用于定义与结果数据数组的第一个样本相对应的物理时间。图 A2 描述了该过程中可用的触发方法之一，我们将在本研究的后面部分使用。

• TRestHitsToTrackProcess: This process takes as input a TRestHitsEvent type and transforms it into a TRestTrackEvent.The hit inter-distances inside the input event are evaluated, and those which fall within a certain distance will be assigned to the same identifiable track.This distance is introduced as a metadata input parameter to the process, named cluster distance.The algorithm starts creating a first track by adding an arbitrary and unassociated hit.The track definition will only end when no more unassociated hits are found to satisfy the inter-distance relation with—and this is important—any of the hits already added to the track, i.e. the inter-distances are evaluated recursively.If after ending the definition of the first track there are still unassociated hits, the process continues to define a second track, and successively.The process ends when no more unassociated hits are found inside the TRestHitsEvent.

主动变更追踪流程:该流程将主动变更追踪类型作为输入，并将其转换为主动变更追踪事件。输入事件内部的命中间隔距离被评估，并且落在某一距离内的那些将被分配到相同的可识别轨迹。该距离作为元数据输入参数引入到流程中，称为集群距离。该算法通过添加任意和不相关的点击开始创建第一个轨迹。只有当没有发现更多未关联的命中满足与已经添加到轨道的任何命中的间距关系时(这一点很重要)，轨道定义才会结束，即间距被递归评估。如果在结束第一首曲目的定义后仍有未关联的命中，则该过程继续定义第二首曲目，并且连续地。当在远程登录中找不到更多未关联的点击时，该过程结束。

See https://sultan.unizar.es/rest/ for further reference.21 As an argument to support this description we assume here that the field drifting the electrons is defined along the z-axis, although the readout plane can be placed in any arbitrary orientation.A hit that does not belong yet to any track.

详情请见 https://sultan.unizar.es/rest/。21 作为支持这种描述的论据，我们在这里假设漂移电子的场是沿着 z 轴定义的，尽管读出平面可以放置在任何任意方向。一首不属于任何轨道的歌曲。

22

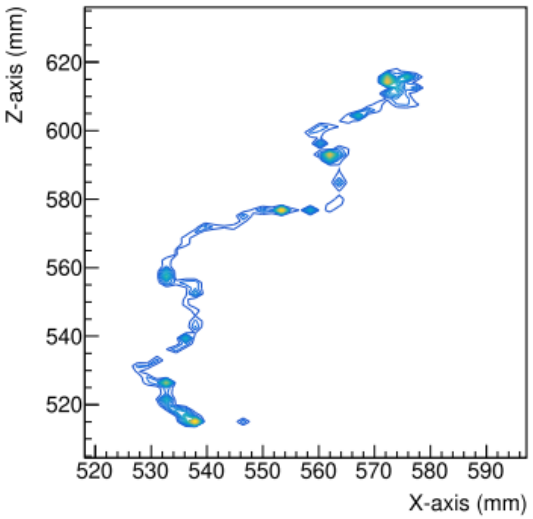
Z-axis (mm)
620
600
580
560
540
520
520 530 540 550 560 570 580 590
X-axis (mm)

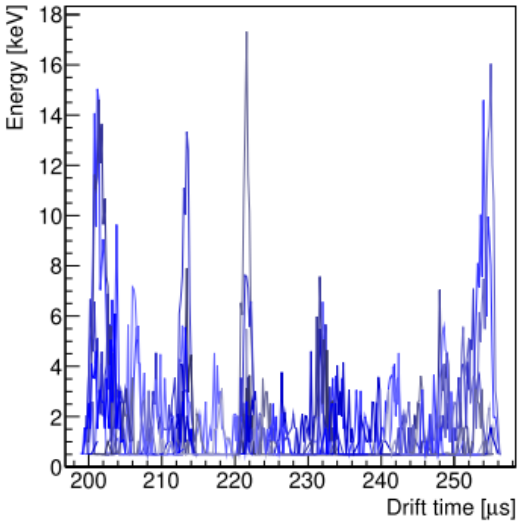
Energy [keV]
18
16
14
12
10
8
6
4
2
0
200 210 220 230 240 250
Drift time [μs]

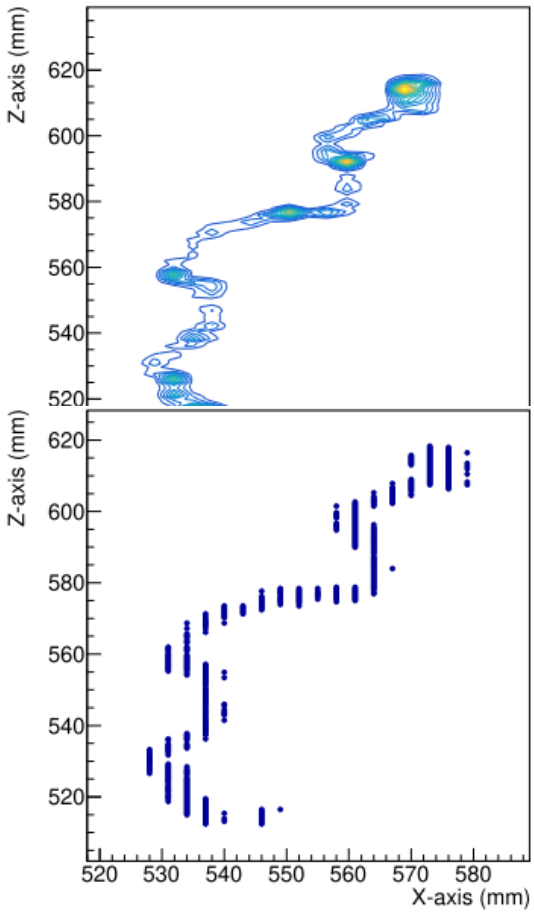
Z-axis (mm)
620
600
580
560
540
520
Z-axis (mm)
620
600
580
560
540
520
520 530 540 550 560 570 580
X-axis (mm)

Figure A1.Representation of different event type outputs after different event processes

图 A1。不同事件过程后不同事件类型输出的表示

on the simulation of a Xe 0νββ event.(a) Top-left panel visualizes a TRestG4Event type, and represents the XZ-plane projection of the charge density of the three-dimensional event.(b) Top-right panel shows a TRestHitsEvent event type after applying the TRestElectronDiffusionProcess where we can appreciate the effect of electron diffusion in a xenon + 1%TMA gas mixture at 10 bar, the readout plane is placed at z = 990 mm. (c) Bottom-left panel shows a TRestTimeSignalEvent type after the conversion by a TRestHitsToSignalProcess.(d) Bottom-right panel shows a TRestHitsEvent type after the reconstruction using TRestSignalToHitsProcess.A scatter plot is used in this case to emphasize the effect introduced by the 3 mm pitch detector readout that can be observed along the x-axis, and the 200 ns sampling rate of the electronics on the z-axis.At this stage the TRestHitsEvent is not anymore a three-dimensional event, since we used here the PandaX-III stripped readout described in appendix B.2.

Xe 0νββ 事件的模拟。(a)左上方的面板显示了一个 trestg 4 事件类型，并表示三维事件电荷密度的 XZ 平面投影。(b)右上方的面板显示了在应用 TresTenceTronDiffusion 过程后的 TRestHitsEvent 事件类型，在此过程中，我们可以理解氙+ 1%TMA 气体混合物在 10 巴下的电子扩散效应，读出平面放置在 z = 990 毫米处。(c)左下方的面板显示了在通过 TRestHitsToSignalProcess 转换后的 TRestTimeSignalEvent 类型。(d)右下方的面板显示了使用 TRestSignalToHitsProcess 重建后的 TRestHitsEvent 类型。在这种情况下，使用散点图来强调沿 x 轴可以观察到的 3 mm 间距检测器读数的影响，以及 z 轴上电子器件的 200 ns 采样速率。在这个阶段，特雷斯脱七不再是一个三维事件，因为我们在这里使用了附录 B.2 中描述的潘达克斯三号剥离读数

23

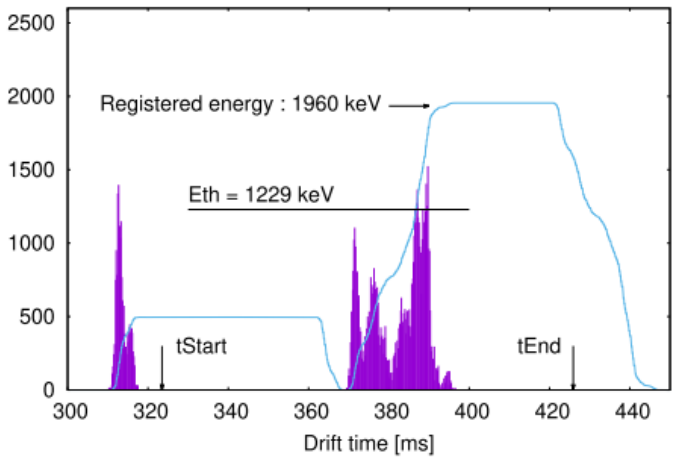

Figure A2.A figure illustrating the trigger definition using the threshold method

图 A2。使用阈值方法说明触发器定义的图

implemented in TRestSignalToRawSignalProcess for a Xe 0νββ event.The filled curve, in red, represents the charge distribution (in arbitrary units not represented on this plot) as a function of the electron drift time.The blue curve is constructed with the integral of the charges (with magnitude represented on the y-axis of this plot) in a fixed time width, here of about ∼50 μs, and corresponding to the half size of the acquisition window of the electronics, of about ∼100 μs. When the integration exceeds a certain

在针对 Xe 0νββ 事件的 TRestSignalToRawSignalProcess 中实现。红色的填充曲线表示电荷分布(以本图中未显示的任意单位表示)作为电子漂移时间的函数。蓝色曲线由固定时间宽度内的电荷积分(幅度表示在该图的 y 轴上)构成，此处约为 50 μs，对应于电子器件采集窗口的一半大小，约为 100 μs。当积分超过一定值时

threshold Eth, in this case equal to Qββ/2 of Xe, the center of the acquisition window is fixed.The resulting acquisition window is represented by tStart and tEnd.An additional offset is introduced on the definition of tStart to assure few time bins will be available for baseline definition during the raw signal event processing.

阈值 Eth，在这种情况下等于 Xe 的 Qββ/2，采集窗口的中心是固定的。最终的采集窗口由 tStart 和 tEnd 表示。在 tStart 的定义中引入了一个额外的偏移，以确保在原始信号事件处理过程中，很少时间槽可用于基线定义。

A.2.2. Hit processes.

A.2.2 .点击流程。

• TRestElectronDiffusionProcess: This process uses the longitudinal and transverse coefficients of a particular gas mixture to emulate the relative deviation of electrons from their original positions in TRestHitsEvent, presumably produced by primary ionization.The energy of each hit found inside the input TRestHitsEvent is converted to the corresponding number of primary electrons that would be produced in the ionization process.Each electron will be a new hit in the output TRestHitsEvent structure, and their coordinates will be randomly deviated following a Gaussian distribution related to the gas parameters, longitudinal and transverse diffusion coefficients, and the distance to the readout plane, which is given as metadata input.The result of applying this process is shown in figure A1(b).This process may optionally add the possibility to include the effect of electron attachment.

远程强扩散过程:该过程使用特定气体混合物的纵向和横向系数来模拟电子从远程强扩散过程中初始位置的相对偏差，这可能是由初级电离产生的。在输入的三重态中发现的每一次碰撞的能量都被转换成电离过程中产生的相应数量的一次电子。每一个电子都将是输出 TRestHitsEvent 结构中的一个新的命中，它们的坐标将按照与气体参数、纵向和横向扩散系数以及到读出平面的距离相关的高斯分布随机偏离，读出平面作为元数据输入给出。应用该过程的结果如图 A1(b)所示。该过程可以选择性地增加包括电子附着效应的可能性。

• TRestHitsSmearingProcess: This process smears the energy of the input TRestHitsEvent according to a Gaussian distribution described by parameters given as metadata input.

特雷斯脱测量过程:该过程根据高斯分布测量输入特雷斯脱的能量，该高斯分布由作为元数据输入给出的参数描述。

A.2.3. Track processes for 0νββ topology.

A.2.3 .跟踪 0νββ 拓扑的过程。

• TRestTrackReductionProcess: This process reduces the number of hits in each of the tracks stored in a TRestTrackEvent, as seen in figure A3(a).An input metadata parameter, Nmax, specifies the maximum number of hits on each of the reduced tracks at the output TRestTrackEvent.The closest hits are merged iteratively till the Nmax condition is satisfied.When two hits are merged, the resulting hit position is calculated weighting the energy of each merged hit.The input parent tracks are also stored in the output TRestTrackEvent, together with the reduced tracks which acquire a relation of inheritance.

TRestTrackReductionProcess:该过程减少了 TRestTrackEvent 中存储的每个轨道的点击数，如图 A3(a)所示。输入元数据参数 Nmax 指定在输出 TRestTrackEvent 中每个缩减轨道上的最大点击数。迭代合并最接近的命中，直到满足 Nmax 条件。当两个命中合并时，计算得到的命中位置加权每个合并命中的能量。输入的父轨道也与获得继承关系的简化轨道一起存储在输出的 TRestTrackEvent 中。

24

J.物理 G: Nucl。部分。《物理》47 (2020) 045108 J Galan 等人

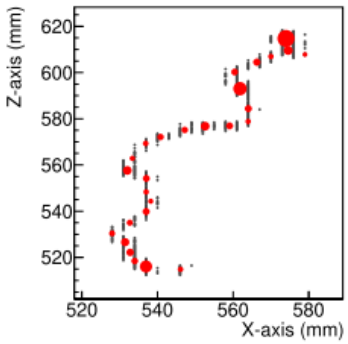

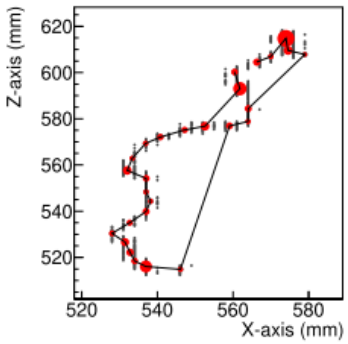

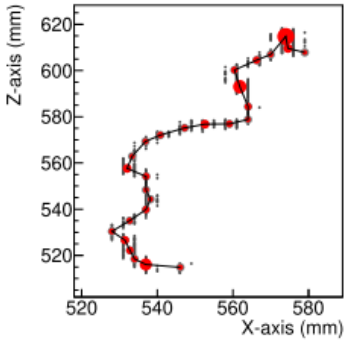

Figure A3.A TRestTrackEvent representation of a Xe 0νββ event after the different track processes used for physical track identification.This event corresponds to the same event used in figure A1.(a) An image of the hit reduction produced by TRestTrackReductionProcess.The red circles represent the final position of reduced hits, which size corresponds with their energy value.The small gray circles on the background represent the hits of the parent track used as input.(b) A polyline is added to this representation to visualize the hits inter-connectivity after the TRestTrackPath-MinimizationProcess.If path minimization works on the whole, it produces at times obviously unphysical connections, as our example illustrates.(c) The unphysical connections are corrected using TRestTrackReconnectionProcess.

图 A3。在用于物理轨道识别的不同轨道过程之后，Xe 0νββ 事件的 TRestTrackEvent 表示。该事件对应于图 A1 中使用的相同事件。(一)减少点击量的图像。红色圆圈代表减少点击的最终位置，其大小与它们的能量值相对应。背景上的灰色小圆圈代表用作输入的父轨道的点击。(b)在该表示中添加一条折线，以显示在追踪路径最小化过程之后的命中互连。如我们的例子所示，如果路径最小化在整体上有效，它有时会产生明显的非物理连接。(c)非物理连接是使用主动跟踪重新连接过程来纠正的。

• TRestTrackPathMinimizationProcess: This process operates only on each of the top-level tracks found in TRestTrackEvent and—using graph theory—finds the shortest path that connects all the hits within each track, as seen in figure A3(b).We have integrated in this process a Held-Karp algorithm [30] optimized for problems that contain between 25 and 35 nodes.This algorithm was extracted from the Concorde travel sales problem libraries

TRestTrackPathMinimizationProcess:该流程仅在 TRestTrackEvent 中找到的每个顶级轨道上运行，并使用图论找到连接每个轨道内所有点击的最短路径，如图 A3(b)所示。我们在这个过程中集成了一个 hold-Karp 算法[30]，该算法针对包含 25 到 35 个节点的问题进行了优化。该算法是从协和式旅行销售问题库中提取的

[31].It is important to notice that the minimization is performed in a closed loop, i.e. the extremes of the physical track are not properly identified at the end of this process.From now on, we will denominate two consecutive hits as connected hits.

[31]。重要的是要注意，最小化是在闭环中执行的，即在此过程结束时，物理轨迹的极值没有被正确识别。从现在开始，我们将把连续两次点击命名为关联点击。

• TRestTrackReconnectionProcess: This process will be commonly used in combination with TRestTrackPathMinimizationProcess.This process will detect unphysical path connections between the hits, or nodes.We understand by unphysical connection a distance between nodes that is larger than the average by a certain number of sigmas, or where no hits from the origin track are found in between, as seen in figure A3(c).The track is split at those unphysical connections and reconnected with the closest hit.Using this technique, the extremes of the physical track are found naturally.Although it was not used in our analysis, this process allows to identify secondary track branches of complex event tracks when reconnection is not possible.

主动跟踪重新连接过程:该过程通常与主动跟踪路径最小化过程结合使用。该过程将检测命中点或节点之间的非物理路径连接。我们通过非物理连接了解到节点之间的距离比平均值大一定数量的 sigmas，或者在节点之间没有发现来自原始轨迹的命中，如图 A3(c)所示。轨道在那些非物质连接处被分开，并与最近的撞击点重新连接。使用这种技术，自然会发现物理轨迹的极端。虽然在我们的分析中没有使用，但是当不可能重新连接时，这个过程允许识别复杂事件轨道的次级轨道分支。

A.2.4. Raw signal processes.

A.2.4 .原始信号处理。

• TRestRawSignalShapingProcess: This process realizes the simulation of the acquisition electronics signal shaper in a TRestRawSignalEvent.It implements the convolution of an analytical response function with the input TRestRawSignalEvent, presumably containing the original charge distribution produced in the detector.The analytical response function requires a single parameter, which is the shaping time.However, this process offers the possibility to introduce any arbitrary wavefunction as response function, adding realism to the generated output.

三重信号整形过程:该过程实现了三重信号事件中采集电子信号整形器的仿真。它实现了分析响应函数与输入信号事件的卷积，可能包含检测器中产生的原始电荷分布。分析响应函数需要单个参数，即成形时间。然而，这一过程提供了引入任意波函数作为响应函数的可能性，为生成的输出增加了真实性。

25

• TRestRawSignalAddNoiseProcess: It is used to include the effect of electronic noise and emulate the fluctuations on the acquired time signal.A value is introduced as input metadata to define the amplitude of the noise.We use a basic noise method implemented in this process that assigns an independent random value, Gaussian distributed, to each of the bins inside a TRestRawSignalEvent.

TRestRawSignalAddNoiseProcess:用于包含电子噪声的影响，并模拟采集的时间信号的波动。引入一个值作为输入元数据来定义噪声的幅度。我们在这个过程中使用了一个基本的噪声方法，它给一个 TRestRawSignalEvent 中的每个面元分配一个独立的随机值，高斯分布。

A.3. The analysis tree

3 .分析树

The different event processes can be combined in sequence to build a more complex pro-cessing chain.In REST, only the event data produced in the last event process will be saved to the output file.There are two main reasons why it is not desirable to stock intermediate event data into a single data file.First, we risk to pile-up, or replicate unnecessarily, data that might require to allocate a non-negligible amount of disk space.Second, the traceability of changes introduced in the data might be lost by storing data at different levels of processing inside a unique file.This possibility would add an undesirable degree of complexity to the future tracking of the data processing, if for example, we decide to continue processing data using a previously processed file with event data at different processing levels but we start our event data processing at an intermediate state.

不同的事件过程可以按顺序组合，以建立一个更复杂的处理链。在 REST 中，只有最后一个事件过程中产生的事件数据才会保存到输出文件中。不希望将中间事件数据存储到单个数据文件中有两个主要原因。首先，我们有堆积或不必要地复制数据的风险，这些数据可能需要分配不可忽略的磁盘空间。第二，通过将数据存储在一个独特的文件中的不同处理级别，数据中引入的变更的可追溯性可能会丢失。这种可能性会给数据处理的未来跟踪增加不必要的复杂性，例如，如果我们决定使用具有不同处理级别的事件数据的先前处理的文件继续处理数据，但是我们在中间状态开始我们的事件数据处理。

However, the inconvenience of this scheme resides on the fact that, during the proces-sing, the event data is transformed in a way that information might be lost, as when we transform a TRestGeant4Event into a TRestHitsEvent.Therefore, it will be not available at the end of the event

data processing.The analysis tree is a REST component that emerges to solve this problem.It is based on a ROOT TTree structure, and it is accessible at any stage of the event data processing by any event process.Any process in REST is allowed to create a new entry, or variable, inside the analysis tree which will be always available in any REST file.Future processing may add new variables to the analysis tree preserving the existing ones from previous processing levels.Therefore, the analysis tree is used to gather relevant information along the processing chain that might not be anymore available at the event data output of the last process.

然而，该方案的不便之处在于，在处理过程中，事件数据的转换方式可能会丢失信息，就像我们将一个 TRestGeant4Event 事件转换为一个 TRestHitsEvent 一样。因此，在事件数据处理结束时，它将不可用。分析树是用来解决这个问题的 REST 组件。它基于 ROOT TTree 结构，并且可以在事件数据处理的任何阶段由任何事件进程访问。REST 中的任何进程都被允许在分析树中创建一个新的条目或变量，该条目或变量在任何 REST 文件中都是可用的。未来的处理可以向分析树添加新的变量，保留先前处理级别的现有变量。因此，分析树用于收集沿处理链的相关信息，这些信息在最后一个过程的事件数据输出中可能不再可用。

In this context, and just for classification purposes, we can distinguish two new types of event processes, the analysis processes and the pure analysis processes.Both type of pro-cesses have in common that they do not modify or transform the input event data, and are just dedicated to add new entries to the analysis tree.Furthermore, the pure analysis processes will not even require access to the event data, being these processes the only ones that can be connected at any place of the processing chain without input/output event type restrictions.For example, a pure analysis process might be a process that reads a variable (or branch) in the analysis tree to perform a multi-peak fit, and write the results of the fit in a metadata structure.

在这种情况下，仅仅为了分类的目的，我们可以区分两种新类型的事件过程，分析过程和纯分析过程。这两种过程的共同之处在于，它们不修改或转换输入事件数据，而只是专门向分析树添加新条目。此外，纯分析过程甚至不需要访问事件数据，因为这些过程是唯一可以在处理链的任何地方连接而没有输入/输出事件类型限制的过程。例如，纯分析过程可能是读取分析树中的变量(或分支)以执行多峰拟合，并将拟合结果写入元数据结构的过程。

Appendix B. PandaX-III Monte Carlo event simulation in REST

附录二:在静止轨道上的潘达克斯-三号蒙特卡罗事件模拟

The first step of Monte Carlo simulation is to consider PandaX-III as a simple calorimeter and simulate the energy deposition of particles interacting in the gaseous medium, or active

蒙特卡罗模拟的第一步是把潘达克斯-3 看作一个简单的量热计，模拟粒子在气体介质或活性物质中相互作用的能量沉积

However, other metadata information used in the processing chain, e.g. process parameters, simulation conditions, readout definition, or gas properties, will be stored without exception, including previous historical metadata information.Although no restrictions apply to produce intermediate files with a snapshot of the event data at a particular step of the processing chain.

然而，在处理链中使用的其他元数据信息，例如过程参数、模拟条件、读出定义或气体属性，将毫无例外地被存储，包括先前的历史元数据信息。尽管在处理链的特定步骤中，没有限制来产生具有事件数据快照的中间文件。

volume of the TPC.The calorimetric response of the conceptual PandaX-III design was studied extensively in [9] using the Geant4-based simulation packages BambooMC and RestG4.In Geant4, detailed tracks of the ionizing particles in the TPC active volume are generated.As a particle travels in the gas medium, it deposits energy along the trajectory via multiple scattering and other physical processes.Geant4 tracks the trajectory in pre-defined steps.In each step, information such as timestamp, particle type, momentum, energy deposition, position, and physical process involved in the interaction are registered.

总容积。在[，使用基于 Geant4 的模拟包 SumbMc 和 RestG4，对概念 PandaX-III 设计的量热响应进行了广泛研究。在 Geant4 中，生成 TPC 有效体积中电离粒子的详细轨迹。当粒子在气体介质中行进时，它通过多次散射和其他物理过程沿着轨道沉积能量。Geant4 以预定义的步骤跟踪轨迹。在每个步骤中，诸如时间戳、粒子类型、动量、能量沉积、位置和交互中涉及的物理过程的信息被记录。

In our study, we use the RestG4 package as an interface to define the simulation con-ditions through a REST metadata structure named TRestG4Metadata, and to store all event information in a TRestG4Event type that can be further processed inside REST, i.e. RestG4 serves to generate a first event dataset.Event tracks can be reconstructed using this original dataset, and we call those MC-true tracks.The MC-true tracks have been generated in Geant4 with a spatial precision of 0.2 mm, implying that every step of the simulation of the movement of a particle is no more than 0.2 mm, with particle information being recorded after each step.The G4EmLivermorePhysics physics list—describing the electromagnetic pro-cesses in Geant4—was used in the event generation.

在我们的研究中，我们使用 RestG4 包作为接口，通过名为 TRestG4 元数据的 REST 元数据结构定义模拟条件，并将所有事件信息存储在 TRESTg4 事件类型中，以便在 REST 中进一步处理，即 RESTg4 用于生成第一个事件数据集。使用这个原始数据集可以重建事件轨迹，我们称这些轨迹为 MC-true 轨迹。在 Geant4 中已经生成了具有 0.2 毫米空间精度的 MC 真实轨迹，这意味着模拟粒子运动的每一步都不超过 0.2 毫米，并且在每一步之后记录粒子信息。G4EmLivermorePhysics 物理列表(描述 Geant4 中的电磁过程)用于事件生成。

The main features of the PandaX-III TPC are faithfully represented in our detector geometry.The cylindrical TPC is 1.5 m in diameter and 2 m in length.The cathode in the middle divides the TPC into two symmetrical drift volumes, in which electrons are drifted away from the cathode and collected by the charge readout planes located at both ends.When running at 10 bar pressure the TPC can hold 200 kg xenon gas.The active volume is con-tained by a 3 cm thick copper vessel, and placed in a water shielding tank in the laboratory.The geometry description, written in GDML [32], is the same as the one used at [9].Therefore, we refer to that publication for further details on the different detector components implemented, materials used, and drawings.

我们的探测器几何形状忠实地反映了潘达克斯-三型热等离子体发生器的主要特征。圆柱形热塑性塑料的直径为 1.5 米，长度为 2 米。中间的阴极将 TPC 分成两个对称的漂移体积，电子从阴极漂移出去，并被位于两端的电荷读出平面收集。当在 10 巴压力下运行时，热动力循环可以容纳 200 公斤氙气。活性体积由一个 3 厘米厚的铜容器容纳，并放置在实验室的水屏蔽罐中。几何描述，写在 GDML [32]，是相同的一个在[9]。因此，我们参考该出版物，了解不同检测器组件的更多细节、使用的材料和图纸。

B.1. Data processing chain for PandaX-III

b . 1 . PanDax-3 的数据处理链

The generated MC-true tracks are introduced in the REST processing scheme to achieve a realistic detector response, including electron drift diffusion, energy resolution, charge readout segmentation, and signal sampling.

在 REST 处理方案中引入生成的真磁迹，以实现真实的探测器响应，包括电子漂移扩散、能量分辨率、电荷读出分段和信号采样。

Figure B1 shows the complete data chain, or event data flow, used to process Geant4 Monte Carlo generated data, and includes different effects related to the detector response.Obvious event type conversion processes detailed in appendix A.2.1, and analysis processes described later on in this chapter, have been omitted in this drawing in order to facilitate focusing on the key aspects of the chain.In our data chain we can differentiate up to three different phases, or stages.In the first phase the event data is conditioned to take into account the physical response of the electrons drifting in the gas medium, in the second phase the readout topology and electronics sampling is considered, and finally in the third phase a physical trackreconstruction takes place to condition the data and make it suitable for a topological track study.The description of event processes required for a full understanding of the processing chain is detailed in appendix A.2.

图 B1 显示了完整的数据链或事件数据流，用于处理 Geant4 蒙特卡罗生成的数据，并包括与探测器响应相关的不同影响。附录 A.2.1 中详述的明显事件类型转换过程和本章下文描述的分析过程在本图中已被省略，以便于关注链的关键方面。在我们的数据链中，我们可以区分多达三个不同的阶段。在第一阶段，事件数据被调整以考虑在气体介质中漂移的电子的物理响应，在第二阶段，考虑读出拓扑和电子采样，最后在第三阶段，发生物理轨迹重建以调整数据并使其适合拓扑轨迹研究。附录 A.2 详细描述了全面理解处理链所需的事件流程

The first phase of the processing takes place exclusively at the TRestHitsEvent level.The input generated by RestG4, encapsulated inside a TRestG4Event type, is transformed into a TRestHitsEvent type using TRestG4ToHitsProcess.Two processes are responsible to include the physical detector response, we use TRestElectronDiffusionProcess to emulate the electron

处理的第一阶段只发生在三层。RestG4 生成的输入被封装在 RestG4 事件类型中，并使用 TRestG4ToHitsProcess 转换为 TRestG4Event 类型。两个过程负责包括物理检测器响应，我们使用远程强扩散过程来模拟电子

We will use the term physical track to refer to the final state of the event reconstruction, where the reconstructed track has physical meaning.

我们将使用术语“物理轨迹”来指代事件重构的最终状态，其中重构的轨迹具有物理意义。

27

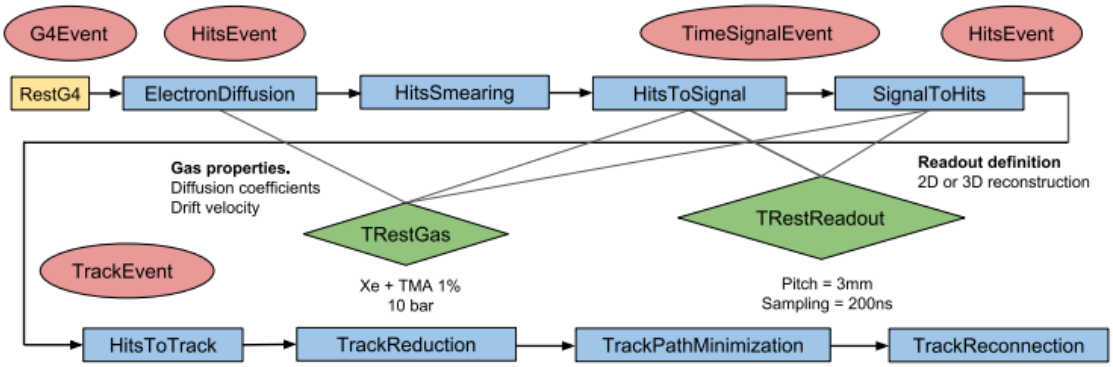

Figure B1.Data processing chain used to manipulate the Monte Carlo events as described in the text.This figure gives an overview of the data flow through the successive event types (red ovals).Few event processes (blue rectangles) have been omitted, for simplicity's sake.The chain starts with Geant4 generated data (yellow rectangle at top-left).The flow is from left to right.We can distinguish two rows of event processes.The top row (TRestElectronDiffusionProcess, TRestHitsToSignalPro-cess, etc) represent processes used to include the detector response (or first phase) and event reconstruction (or second phase), while the bottom row represents the track processes used for physical track reconstruction (or third phase).Just in this figure, the TRest prefix and Process termination has been removed from the REST process and event names.

图 B1。用于操纵蒙特卡罗事件的数据处理链，如本文所述。此图概述了连续事件类型(红色椭圆)中的数据流。为了简单起见，很少忽略事件过程(蓝色矩形)。链从 Geant4 生成的数据开始(左上角的黄色矩形)。流量从左到右。我们可以区分两行事件进程。最上面一行(TRestElectronDiffusionProcess、TresItestOsatalProcess 等)表示用于包括检测器响应(或第一阶段)和事件重建(或第二阶段)的过程，而最下面一行表示用于物理轨道重建(或第三阶段)的轨道过程。就在这个图中，从 Rest 进程和事件名称中删除了 TRest 前缀和进程终止。

diffusion in the gaseous medium, and TRestHitsSmearingProcess to include the stochastic effect of the detector energy resolution on each independent event.The gas properties used in TRestElectronDiffusionProcess were obtained from Magboltz [33] through the Garfield+ +[28] interface integrated in TRestGas.In our study we used a gas mixture of xenon+1% TMA at 10bar pressure, setting the TPC drift field to 1 kV cm−leads to an electron drift velocity of 1.86 mm µs −, and 1.46 × 10−cm/and 1.01 × 10−cm/, for the long-itudinal and transverse electron diffusion coefficients, respectively.The number of primary electrons yielded at each deposition is correlated with the energy deposited according to the work-function, or W-value, i.e. the energy required to extract an electron from an atom.We use a W-value of 21.9 eV [34] for our gas mixture.The detector energy resolution introduced in TRestHitsSmearingProcess was defined as 3%-FWHM at Qββ = 2 457.83 keV.

气体介质中的扩散，以及包括探测器能量分辨率对每个独立事件的随机影响的三重测量过程。特雷斯特强扩散过程中使用的气体特性是通过集成在特雷斯特加斯的加菲尔德+ +[28]接口从[33]获得的。在我们的研究中，我们使用氙+1% TMA 的气体混合物，在 10 巴压力下，将 TPC 漂移场设置为 1 千伏厘米，导致电子漂移速度分别为 1.86 毫米 µs、1.46 × 10 厘米/和 1.01 × 10 厘米/的纵向和横向电子扩散系数。根据功函数或 W 值，即从原子中提取电子所需的能量，每次沉积产生的一次电子的数量与沉积的能量相关。我们使用 21.9 电子伏[34]的瓦特值作为我们的气体混合物。探测器能量分辨率被定义为 3%-FWHM，Qββ = 2 457.83 keV。

During the second phase the conversion processes TRestHitsToSignalProcess and TRestSignalToHitsProcess are responsible to introduce the detector granularity and electro-nics sampling of the time signal induced on the detector readout.These processes are strongly dependent on the TRestReadout definition, detailed in appendix B.2. For now, it is enough to mention that

TRestHitsToSignalProcess discretizes our event data into time signals in steps of 200 ns, using a two-dimensional readout of 3 mm pitch.At this stage, other details related to time signal conditioning could be added, despite the fact that it is not the aim of this work to include those effects, and any future improvement will be later discussed in our final con-clusions.Then, TRestSignalToHitsProcess reconstructs the event recovering the TRestHit-sEvent structure including the effects introduced by the previous process, as it is shown in figure A1(d).

在第二阶段期间，转换过程 TRestHitsToSignalProcess 和 TRestSignalToHitsProcess 负责引入检测器粒度和检测器读数上感应的时间信号的电子采样。这些过程强烈依赖于特雷斯脱定义，详见附录 B.2。目前，只要提到特雷斯脱信号过程就足够了，它使用 3 毫米间距的二维读数，将我们的事件数据离散为 200 纳秒的时间信号。在此阶段，可以添加与时间信号调节相关的其他细节，尽管事实上本工作的目的并不是要包括这些影响，任何未来的改进将在我们的最终结论中讨论。然后，TRestSignalToHitsProcess 重构恢复 trestIt-sEvent 结构的事件，包括前一个过程引入的效果，如图 A1(d)所示。

28

In the final third phase, the reconstructed TRestHitsEvent is classified into tracks through the TRestHitsToTrackProcess using a cluster distance value of 7.5 mm, i.e. two tracks are considered to be independent if the closest hits distance from one track to another is above 7.5 mm. In this phase the processes described in appendix A.2.3 are used to determine the physical track, evaluating the hit distances and connectivity.Figure A3 shows the result of the three track processes implemented in this phase of the processing chain;TRest-TrackReductionProcess (where we use Nmax = 35), TRestTrackPathMinimizationProcess and TRestTrackReconnectionProcess.At the end of this processing chain we end up with a reconstructed physical track where track ends can be recognized naturally.It is the respon-sibility of the analysis processes to extract information, or observables, along the data pro-cessing chain, to be used in a final pattern recognition analysis.

在最后的第三阶段，使用 7.5 毫米的聚类距离值，将重建的特雷斯脱七条轨道通过特雷斯脱-特雷斯脱图 A3 显示了在处理链的这一阶段实施的三个跟踪过程的结果；TRest-TrackReductionProcess(我们使用 Nmax = 35)、TresTrackPathMinimizationProcess 和 TRestTrackReconnectionProcess。在这个处理链的末端，我们以一个重建的物理轨迹结束，在这里轨迹末端可以被自然地识别。分析过程的责任是沿着数据处理链提取信息或观察值，用于最终的模式识别分析。

It is important to remark that the event data processing chain discussed here is fully compatible with two and three-dimensional event representation, i.e. a TRestHitsEvent structure is able to identify if it contains 2D or 3D hits, and the hit and track processes will act on the event data accordingly, e.g. TRestTrackPathMinimizationProcess will independently minimize the paths of different projections and tracks produced by a two-dimensional readout.Ultimately, it is the sole responsibility of the TRestReadout metadata structure to define the topological nature of the event data.

值得注意的是，这里讨论的事件数据处理链与二维和三维事件表示完全兼容，也就是说，一个三重结构能够识别它是否包含 2D 或三维命中，并且命中和跟踪过程将相应地作用于事件数据，例如，三重跟踪路

径最小化过程将独立地最小化由二维读出产生的不同投影和轨道的路径。最终，定义事件数据的拓扑性质是 TRestReadout 元数据结构的唯一责任。

B.2. PandaX-III readout metadata description

B.2. PandaX-III 读出元数据描述

For charge readout, PandaX-III baseline design relies on Microbulk Micromegas technology due to its good intrinsic radiopurity levels, good energy resolution and capability to operate at high pressure [12, 13].A modular design has been conceived to build each detector readout plane in the PandaX-III TPC design due to the Microbulk size limitation imposed by its fabrication process.In order to cover the full active area of the detector, each readout plane consists of 41 independent Micromegas modules, as shown in figure B2(a).The total number of acquisition channels is limited to a manageable level by physically interconnecting pixels along the horizontal or vertical axis orientations and they are read out as a single readout channel, or strip, as shown in figure B2(b).Each Micromegas module contains 64 X-strips and 64 Y-strips of 3 mm pitch.

对于电荷读出，PandaX-III 基线设计依赖于 Microbulk Micromegas 技术，因为它具有良好的内在辐射安全水平、良好的能量分辨率和在高压下工作的能力[12，13]。由于制造工艺对微球尺寸的限制，已设想采用模块化设计来构建 PandaX-III 热防护板设计中的每个探测器读出平面。为了覆盖探测器的全部有效区域，每个读出平面由 41 个独立的微兆模块组成，如图 B2(a)所示。通过沿水平或垂直轴方向物理互连像素，采集通道的总数被限制在可管理的水平，并且它们作为单个读出通道或条被读出，如图 B2(b)所示。每个微兆模块包含 64 个 3 毫米间距的 X 带和 64 个 Y 带。

The integration of a realistic complex readout scheme in REST is done through the TRestReadout metadata structure.TRestReadout is a sophisticated structure that defines an arbitrary number of readout planes, containing itself any number of readout modules composed of readout channels that are identified with the DAQ channels registered by the electronics.A readout channel itself is built of one or more readout pixels.A readout pixel is the most elementary component of the readout description in REST, and it defines its position relative to the module coordinates, its size, orientation, and shape.The combi-nation of readout pixels with different sizes, orientations, and shapes at different positions allows to construct any desired readout topology in REST.

在 REST 中集成一个实际的复杂读出方案是通过 TRestReadout 元数据结构完成的。TRestReadout 是一种复杂的结构，它定义了任意数量的读出平面，包含由读出通道组成的任意数量的读出模块，这些读出通道由电子设备记录的 DAQ 通道识别。读出通道本身由一个或多个读出像素构成。读出像素是 REST 中读出描述的最基本组成部分，它定义了相对于模块坐标的位置、大小、方向和形状。在不同位置具有不同尺寸、方向和形状的读出像素的组合允许在 REST 中构建任何期望的读出拓扑。

Different methods are available at TRestReadout and related classes to access the readout description, and determine for a given hit coordinates which is the corresponding readout channel in an efficient way.These methods are accessed by related event processes and they are exploited to translate a given TRestHitsEvent coordinates into TRestTimeSignalEvent channels, and vice versa.The TRestReadout definition is a crucial element in the construction

在 TRestReadout 和相关类中有不同的方法来访问读出描述，并以有效的方式确定给定命中坐标的相应读出通道。这些方法由相关的事件进程访问，它们被用来将给定的 TRestHitsEvent 坐标转换为 trestItems 信号事件通道，反之亦然。TRestReadout 定义是构造中的一个关键元素

Mainly due to the existing equipment used for production.27 Readout channel reduction plays an important role to simplify the design, reduce costs and minimize the impact of typically non-clean

electronics from the radiopurity point of view, on a detector component that must be placed as close as possible to the readout plane to minimize electronic noise induction on the readout signal.

主要是由于现有设备用于生产。27 读出通道的减少对于简化设计、降低成本和最小化从辐射安全角度来看典型的非清洁电子器件对探测器组件的影响起着重要作用，探测器组件必须尽可能靠近读出平面放置，以最小化读出信号上的电子噪声感应。

29

29

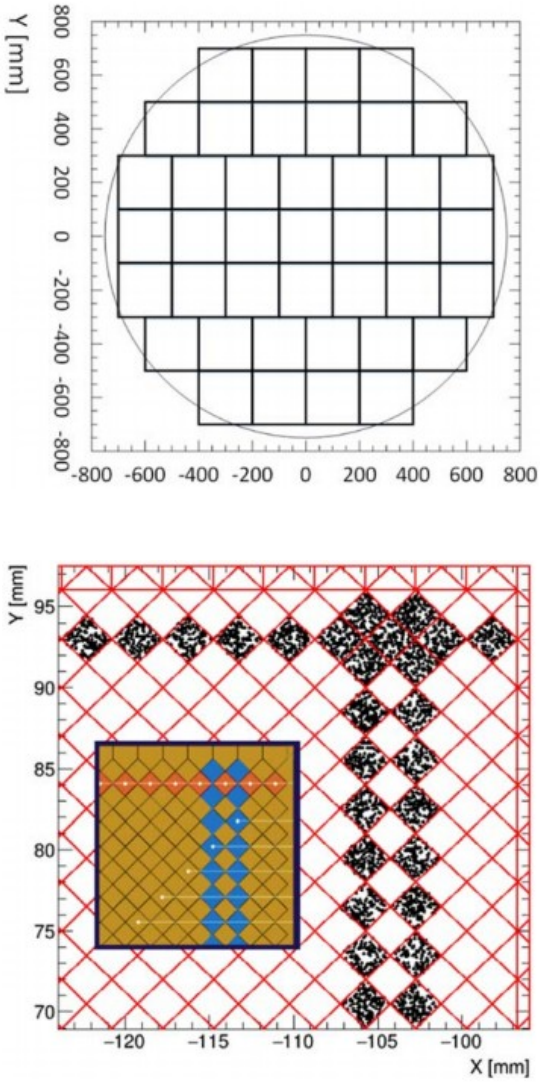

Figure B2.(a) The PandaX-III readout plane description in REST, built using 41 Micromegas modules of size 192 mm × 192 mm. The circle of size R = 75 cm defines

图 B2。(a)在 REST 中的 PandaX-III 读出平面描述，使用 41 个尺寸为 192 毫米× 192 毫米的微兆模块构建。尺寸为 R = 75 厘米的圆定义

the inner radius where the Xe gas is contained.The active detector area is formed by the region of the modules found inside that circle.Small corners inside this circular region are not covered by any readout module, and therefore, they will translate into a signal efficiency loss in our final detector response.(b) The detail of a Micromegas readout module region as implemented in REST, red lines define the limits of readout pixels.Two readout channels on the X-axis and one readout channel on the Y-axis are drawn (black dots) using REST readout validation routines, which allow to select, or activate, a group of readout channels and—after generating a number of random coordinates—paint only those generated coordinates that are found inside the active channels.The small embedded image is the corresponding area extracted from the original Gerber design used for fabrication.The Gerber representation has been modified to identify the two X-axis (blue pixels) and one Y-axis (orange pixels) readout channels active for the readout validation.

包含 Xe 气体的内径。活动探测器区域由该圆内的模块区域构成。这个圆形区域内的小角落没有被任何读出模块覆盖，因此，它们将转化为最终检测器响应中的信号效率损失。微兆读出模块区域的细节如在 REST 中实现的，红线定义读出像素的界限。使用 REST 读出验证例程绘制 X 轴上的两个读出通道和 Y 轴上的一个读出通道(黑点)，该例程允许选择或激活一组读出通道，并在生成多个随机坐标后，仅绘制在活动通道内找到的那些生成的坐标。小嵌入图像是从用于制造的原始 Gerber 设计中提取的相应区域。对 Gerber 表示法进行了修改，以识别两个 X 轴(蓝色像素)和一个 Y 轴(橙色像素)读出通道，用于读出验证。

of the data processing chain and its generic implementation provides versatility to study a common dataset with different detector readout topologies and granularities, as it is done in section 3.

数据处理链及其通用实现提供了研究具有不同探测器读出拓扑和粒度的公共数据集的通用性，如第 3 节所述。

In particular, the two-dimensional stripped baseline readout for PandaX-III cannot perform an unequivocal three-dimensional reconstruction of the original event topology (see discussion at [24]).In our design, a drifted electron that reaches a Micromegas module will induce a signal on either a X-strip or a Y-strip.Therefore, the TRestHitsEvent reconstruction after TRestSignalToHitsProcess is necessarily a combination of two-pro-jections, a projection formed by XZ-hits (i.e. hits with valid X and Z coordinates and undefined Y coordinate) derived from signals corresponding to the X-strips, and a pro-jection formed by YZ-hits resulting from the signals found at Y-strips.Figure B3 shows the resulting projections for a signal and a background event.End-track identification using the analysis processes described in the following subsection have been also represented in this figure.The main characteristics of signal and background events is discussed in section 2.1.

特别是，PandaX-III 的二维剥离基线读数不能对原始事件拓扑进行明确的三维重建(见[24 的讨论)。在我们的设计中，一个漂移的电子到达一个微波模块时，会在一个 X 带或一个 Y 带上感应出一个信号。因此，在 TRestSignalToHitsProcess 之后的 TRestHitsEvent 重建必然是两个投影的组合，一个投影由从对应于 X 条的信号中导出的 XZ 命中(即具有有效的 X 和 Z 坐标以及未定义的 Y 坐标的命中)形成，另一个投影由在 Y 条处发现的信号中得到的 YZ 命中形成。图 B3 显示了信号和背景事件的投影结果。下图中还显示了使用下一小节中描述的分析过程进行的最终轨迹识别。第 2.1 节讨论了信号和背景事件的主要特征。

30

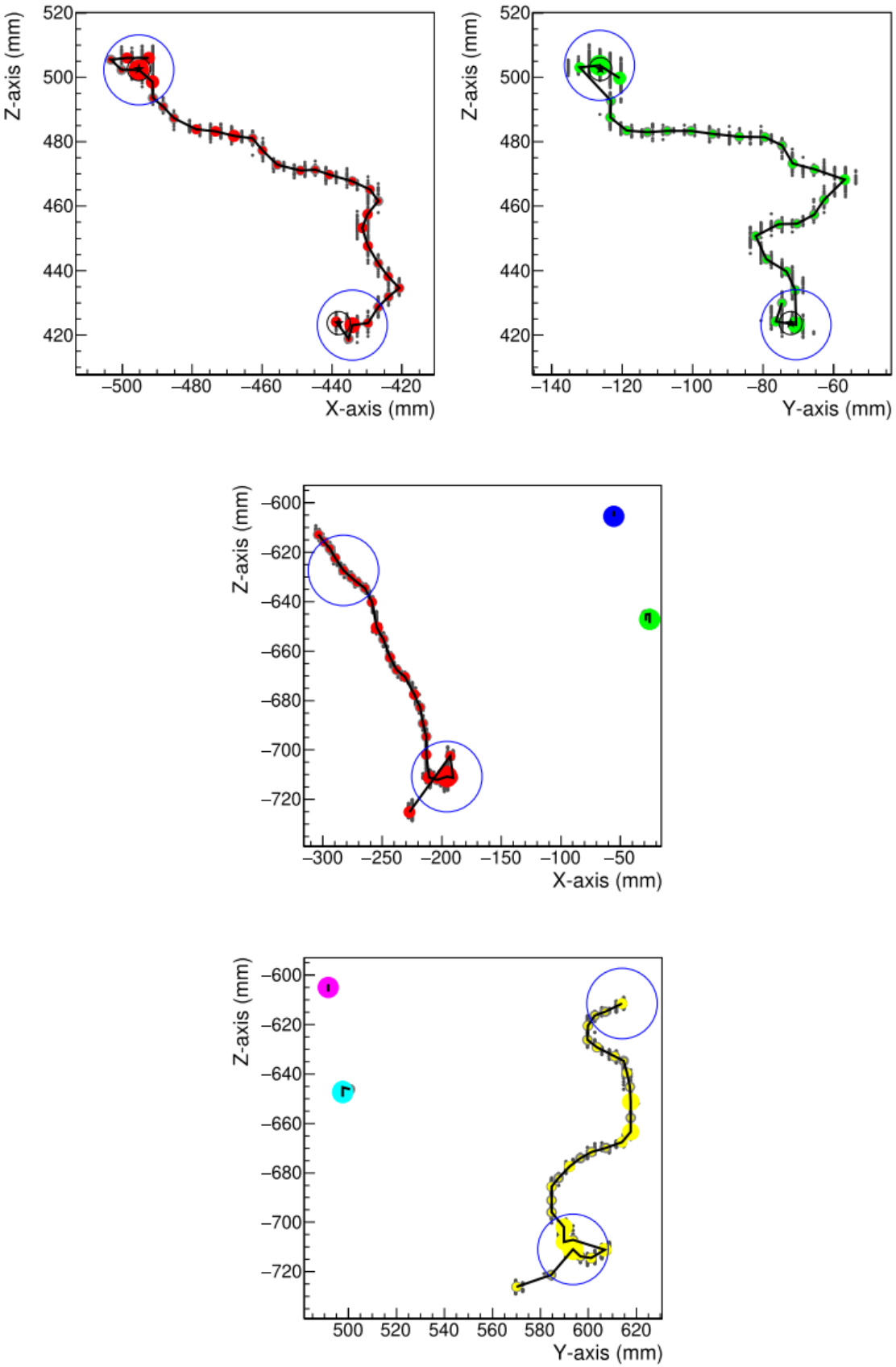

Figure B3.A TRestTrackEvent representation of the two-dimensional projected electron tracks for a 0νββ (a) and a background event produced in the U decay chain (b) at the end of the data processing chain.The colored filled circles correspond to the top-level track of a TRestTrackEvent, while the gray scattered points in the background —where the 3 mm pitch granularity can be discerned— represent the hits in the origin track.The size of the circle in the top-level tracks is proportional to

the hit energy, and different colors serve to identify independent tracks classified after the TRestHitsTo-TrackProcess.A black polyline shows the top-level track hits interconnectivity resulting after the TRestTrackReconnectionProcess, and helps to visualize the physical track.Large blue circles correspond with our blob charge definition (R = 12 mm) obtained from TRestFindTrackBlobsProcess, described in appendix B.3. The starred black markers found in the 0νββ event correspond with the positions obtained from the TRestFindG4BlobProcess representing the last electron energy deposition for each of the primary simulated electron tracks.

图 B3。在数据处理链末端的铀衰变链(b)中产生的 0νββ (a)和背景事件的二维投影电子轨道的一种 TRestTrackEvent 表示。彩色实心圆对应于 TRestTrackEvent 的顶层轨道，而背景中的灰色分散点(可以分辨出 3 mm 间距)代表原始轨道中的命中。顶层轨道中的圆的大小与击中能量成比例，不同的颜色用于识别在特雷斯托-轨道过程之后分类的独立轨道。黑色多段线显示了在跟踪重新连接过程后产生的顶层跟踪命中互连，并有助于可视化物理跟踪。大的蓝色圆圈对应于我们的斑点电荷定义(R = 12 毫米)，该定义是从 TRestFindTrackBlobsProcess 获得的，如附录 B.3 所述。在 0νββ 事件中发现的带星号的黑色标记对应于从 TRestFindG4BlobProcess 获得的位置，该位置代表每个初级模拟电子轨道的最后电子能量沉积。

31

B.3. Analysis event processes

B.3 .分析事件流程

Additional event processes are used during the data processing chain in order to extract required event information in our posterior analysis.The analysis processes used, the place of the processing chain where those processes are used, the particular information extracted and/ or other parameters required are detailed in the following list.

在数据处理链中使用额外的事件过程，以便在我们的后验分析中提取所需的事件信息。使用的分析过程、使用这些过程的处理链的位置、提取的特定信息和/或所需的其他参数在下面的列表中详细列出。

• TRestFindG4BlobProcess: It is used at the beginning of the first phase of the data processing chain.It operates in a TRestG4Event and it is used to extract the MC-true track coordinates of each electron track end in a 0νββ event.These values are used to assess the goodness of our algorithms to identify the track ends after the physical event reconstruction.

主动变更 4BlobProcess:在数据处理链的第一阶段开始时使用。它在 TRESTg 4 事件中运行，用于提取 0νββ 事件中每个电子轨道末端的真轨道坐标。这些值用于评估我们的算法在物理事件重建后识别轨迹终点的优劣。

• TRestG4AnalysisProcess: It is also used at the beginning of the data chain, after the previous process.This process is used to add different observables related with the TRestG4Event to the analysis tree, as e.g. the interaction types involved, or the number and type of particles involved in the event.In our particular case we use this process to extract the total energy deposited in the active volume of the detector, without any fiducialization.

TRestG4AnalysisProcess:它也用于数据链的开头，在前面的过程之后。该过程用于将与 TRESTg 4 事件相关的不同观察值添加到分析树中，例如所涉及的相互作用类型，或事件中所涉及的粒子数量和类型。在我们的特殊情况下，我们使用这一过程提取探测器有效体积中沉积的总能量，而没有任何基准化。

• TRestTriggerAnalysisProcess: It is used at the second phase of the processing chain, at the TRestTimeSignalEvent level.This process uses the same trigger definition implemented in TRestSignalToRawSignalProcess shown previously in figure A2.We apply a sampling rate of 5 MHz with a total number of 512 sampled points, as fixed by the PandaX-III electronics system, and a trigger energy threshold, Eth, of 1229 keV corresponding to Qββ/2.This process generates a new observable in the analysis tree, defining the energy contained in the virtual acquisition window defined.It must be noted that this process, as any other analysis process, does not modify the event data.

TRestTriggerAnalysisProcess:它用于处理链的第二阶段，即 TRestTimeSignalEvent 级别。该过程使用与图 A2 所示的 TRestSignalToRawSignalProcess 中实现的触发器定义相同的触发器定义。我们采用 5 MHz 的采样速率，总共 512 个采样点，由 PandaX-III 电子系统固定，触发能量阈值 Eth 为 1229 keV，对应于 Qββ/2。该过程在分析树中生成一个新的可观察值，定义包含在所定义的虚拟采集窗口中的能量。必须注意的是，该过程与任何其他分析过程一样，不会修改事件数据。

• TRestTrackAnalysisProcess: It is used at the end of the third phase of the processing chain.It extracts parameters used for pattern recognition of 0νββ events, such as the number of tracks, the track energy ratio, or the twist parameter described in section 2.1.

TRestTrackAnalysisProcess:在处理链的第三阶段结束时使用。它提取用于 0νββ 事件模式识别的参数，如轨道数量、轨道能量比或第 2.1 节中描述的扭曲参数。

• TRestFindTrackBlobsProcess: It is also used at the end of the processing chain.The tracks ends have been naturally identified after the TRestTrackReconnectionProcess, and this process registers the coordinates or positions of the end-tracks in the analysis tree.This process searches for the highest density region within a 20% of the track length at the track end, in order to allow an additional degree of freedom identifying the final blob position.This process is used to generate the observables related to the blobs charge parameter, described in section 2.1.

TRestFindTrackBlobsProcess:它也用于处理链的末端。在跟踪重连过程之后，轨迹末端被自然地识别，并且该过程在分析树中记录末端轨迹的坐标或位置。该过程在轨道末端的轨道长度的 20%内搜索最高密度区域，以便允许识别最终斑点位置的额外自由度。该过程用于生成与斑点电荷参数相关的可观测值，如第 2.1 节所述。

Appendix C. Full Monte Carlo detector response

附录三:蒙特卡罗探测器的完整响应

In order to test the detector's capability to distinguish surface events we need to extract a new parameter connected with the diffusion of electrons, from the event data processing chain presented in appendix B.1. We could extract such a parameter at different stages in that chain, however, a straightforward parameter characterizing the spread of the charge is the width of the pulses as recorded by the readout electronics.We require then additional event processing to accommodate our Monte Carlo generated events to a time signal similar to the recorded with the detector acquisition.Figure C1 shows the additional event processes, detailed also in appendix A.2, that we have introduced after TRestHitsToSignalProcess, at the second phase of the data chain described in appendix B.1.

为了测试探测器区分表面事件的能力，我们需要从附录 B.1 中的事件数据处理链中提取一个与电子扩散相关的新参数。我们可以在该链的不同阶段提取这样一个参数，但是，表征电荷扩散的一个直接参数是读出电子记录的脉冲宽度。然后，我们需要额外的事件处理，以将我们的蒙特卡罗生成的事件调整为类似于探测器采集记录的时间信号。图 C1 显示了额外的事件过程，在附录 A.2 中也有详细说明，我们在数据链的第二阶段，在附录 B.1 中描述的数据链中引入了 TRestHitsToSignalProcess

32

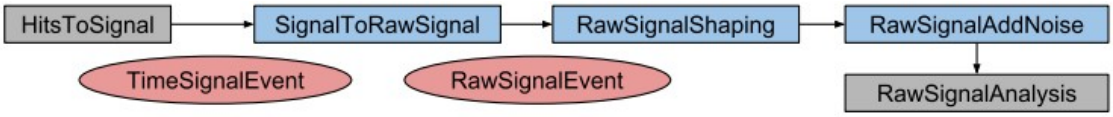

Figure C1.Extension of the event data chain to include appropriate detector readout signal conditioning, trigger definition, electronics shaping and electronic noise.The first process TRestHitsToSignalProcess—inside the first gray box—corresponds to the process shown previously in figure B1.The event processing ends with the TRestRawSignalAnalysisProcess after we extract the parameters of interest for the fiducial analysis carried out in section 4.The TRest prefix and Process termination has been removed from the REST process and event names, keeping the same nomenclature as in figure B1.

图 C1。事件数据链的扩展，包括适当的检测器读出信号调节、触发定义、电子整形和电子噪声。在第一个灰色框中的第一个流程 TRestHitsToSignalProcess 对应于前面图 B1 所示的流程。在我们为第 4 节中执行的基准分析提取了感兴趣的参数之后，事件处理以 TRestRawSignalAnalysisProcess 结束。TRest 前缀和进程终止已经从 Rest 进程和事件名称中移除，保持与图 B1 中相同的命名。

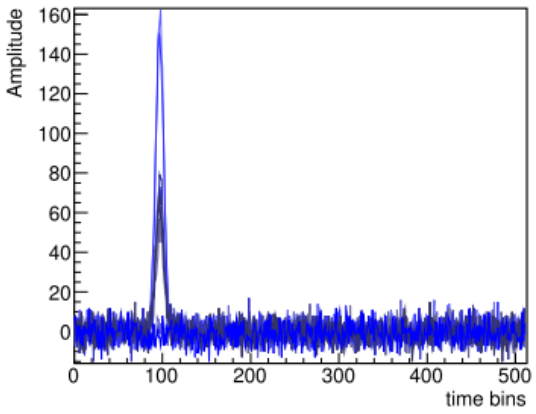

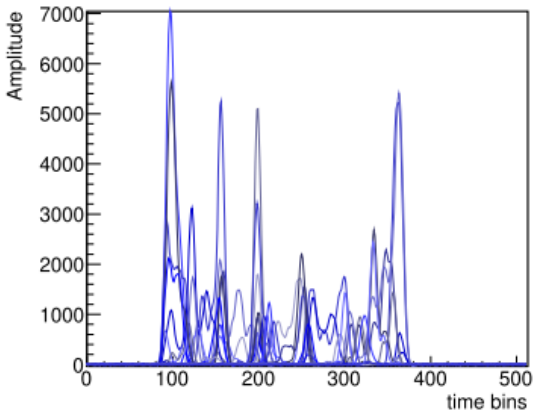

Figure C2.A TRestRawSignalEvent representation after applying the event processes present on the signal conditioning data chain, including trigger definition, electronics shaping and electronic noise contributions.(a) The readout signals for a 10 keV electron generated in the middle of our TPC volume, at z = 500 mm. (b) The readout signals for a 0νββ signal event.

图 C2。在应用信号调节数据链上出现的事件过程之后的一种主动信号事件表示，包括触发定义、电子整形和电子噪声贡献。(a)10 keV 电子的读出信号产生于我们的热等离子体体积的中部，z = 500 毫米，(b)0νββ 信号事件的读出信号。

In this extension of the processing chain we transform our event data into a TRes-tRawSignalEvent where we introduce different effects on the detector response, as a semi-Gaussian electronic signal shaper with 1 μs peaking time and a Gaussian noise level, at each channel.In order to adjust the noise level we have simulated a small energetic deposition, produced by a 10 keV electron, and we have chosen the noise level that approximately reproduces our signal-to-noise values when taking data in normal laboratory conditions.The unit values at this stage are completely arbitrary.Figure C2 shows the aspect of the final processed event after including all these effects.

在处理链的这一扩展中，我们将事件数据转换为 TRes-tRawSignalEvent，在这里我们引入了对检测器响应的不同影响，作为半高斯电子信号整形器，在每个通道具有 1 μs 的峰值时间和高斯噪声水平。为了调整噪声水平，我们模拟了一个由 10 keV 电子产生的小能量沉积，并且我们选择了在正常实验室条件下采集数据时近似再现信噪比值的噪声水平。这个阶段的单位值完全是任意的。图 C2 显示了包含所有这些影响后的最终处理事件的情况。

These additional effects are included at the TRestRawSignalEvent level to gain realism, but at the same time to exploit the REST analysis process, TRestRawSignalAnalysisProcess, which is also used to analyze the real data of the detector.This analysis process is used right after TRestRawSignalAddNoiseProcess to extract the diffusion parameter that we are interested in.In order to define our diffusion parameter, σw, we pre-select those channels exceeding a certain energy threshold measured in signal amplitude at the TRestRawSignalEvent.The threshold value is defined as the 10% of the maximum amplitude found inside the TRestRawSignalEvent.Then, we obtain the FWHM of the maximum peak at each channel, and average the 9 channels which

这些额外的效果包含在 TRestRawSignalEvent 级别以获得真实性，但同时利用 REST 分析过程，TRestRawSignalAnalysisProcess，它也用于分析探测器的真实数据。这个分析过程在 TRestRawSignalAddNoiseProcess 之后被用来提取我们感兴趣的扩散参数。为了定义我们的扩散参数 σw，我们预先选择那些超过某个能量阈值的通道，该能量阈值是在 TRestRawSignalEvent 的信号幅度中测量的。阈值被定义为在 TRestRawSignalEvent 内发现的最大振幅的 10%。然后，我们得到每个通道的最大峰值的 FWHM，并平均 9 个通道

33

produce the lowest FWHM values.The value of σw is measured in samples, or bins, of 200 ns width which is the sampling value we used in the detector response.

产生最低的 FWHM 值。σw 的值以 200 ns 宽度的样本或箱来测量，这是我们在检测器响应中使用的采样值。

ORCID iDs

ORCID iDs

J Galan https://orcid.org/0000-0001-7529-9834 C Fu https://orcid.org/0000-0002-0031-2077

加兰·https://orcid.org/0000-0001-7529-9834·https://orcid.org/0000-0002-0031-2077

References

参考

[1] Fukuda Y et al 1998 Evidence for oscillation of atmospheric neutrinos Phys. Rev. Lett.81 15627

[1]福田康夫等 1998 大气中微子振荡的证据物理版列特。81 15627

[2] Ahmad Q R et al 2002 Direct evidence for neutrino flavor transformation from neutral current interactions in the Sudbury neutrino observatory Phys. Rev. Lett.89 011301

[2]艾哈迈德·奎尔等人 2002 年在萨德伯里中微子观测站物理版列特中从中性电流相互作用中得到的中微子味转化的直接证据。89 011301

[3] Majorana E and Majorana E 1937 Nuovo Cimento 14 171

[3]马略纳东和马略纳东 1937 诺沃西门托 14 171

[4] Barabash A S 2010 75 years of double beta decay: yesterday, today and tomorrow DAE Symp.Nucl.Phys. 55 I13

[4]巴拉巴什 2010 年 75 年的双 β 衰变:昨天，今天和明天的 DAE 症状。努克尔。Phys. 55 I13

[5] Dell'Oro S, Marcocci S, Viel M and Vissani F 2016 Neutrinoless double beta decay: 2015 review Adv. High Energy Phys. 2016 2162659

[5]2016 年无中微子双 β 衰变:2015 年回顾高级高能物理学 2016 2162659

[6] Schechter J and Valle J W F 1982 Neutrinoless double beta decay in SU(2) x U(1) theories Phys. Rev. D 25 2951

[6]谢切特和瓦莱 1982 无中微子双 β 衰变在 SU(2) x U(1)理论物理 Rev. D 25 2951

Schechter J and Valle J W F 1981 Phys. Rev. D 25 289

《1981 年物理学报》第 25 卷第 289 期

[7] Avignone F T III, Elliott S R and Engel J 2008 Double beta decay, Majorana neutrinos, and neutrino mass Rev. Mod.Phys. 80 481

[2008 双 β 衰变，马略纳中微子和中微子质量修正模型。Phys. 80 481

[8] Agostini M, Benato G and Detwiler J 2017 Discovery probability of next-generation neutrinoless double-beta decay experiments Phys. Rev. D 96 053001

[2017 下一代无中微子双 β 衰变实验的发现概率

[9] Chen X et al 2017 PandaX-III: searching for neutrinoless double beta decay with high pressure 136 Xe gas time projection chambers Sci.China Phys. Mech.Astron.60 061011

[9]陈 X 等 2017 潘大三:用高压 136 Xe 气体时间投影室寻找无中微子双 β 衰变。中国物理机械。阿斯顿。60 061011

[10] Li J, Ji X, Haxton W and Wang J S Y 2015 The second-phase development of the China JinPing underground laboratory 13th Int.Conf.on Topics in Astroparticle and Underground Physics, TAUP 2013.;Phys. Proc.61 57685

2015 中国金平地下实验室二期开发第 13 届国际。糖膏剂关于天体粒子和地下物理学的主题，TAUP 2013。；物理过程。61 57685

[11] Redshaw M, Wingfield E, McDaniel J and Myers E G 2007 Mass and double-beta-decay Q value

[11]瑞德肖 M，温菲尔德 E，麦克丹尼尔 J 和迈尔斯 2007 年质量和双 β 衰变 Q 值

of Xe Phys. Rev. Lett.98 053003

列特物理牧师。98 053003

[12] González-Díaz D et al 2015 Accurate γ and MeV-electron track reconstruction with an ultra-low diffusion Xenon/TMA TPC at 10 atm Nucl.Instrum.Methods Phys. Res. A 804 824

[12]冈萨雷斯-迪亚斯 D 等人 2015 年精确的 γ 和兆电子伏电子轨道重建与超低扩散氙/三甲氧基三甲基氯化铵在 10 个大气压核。仪器。方法物理文献 A 804 824

[13] Lin H et al 2018 Design and commissioning of a 600 L time projection chamber with Microbulk Micromegas J. Instrum.13 P06012

[13]林宏等 2018 设计和调试了一个 600 升的时间投影室。13 P06012

[14] Andriamonje S et al 2010 Development and performance of Microbulk Micromegas detectors J. Instrum.5 P02001

[14] Andriamonje S 等 2010 微球微兆探测器的发展和性能。5 P02001

[15] Vuilleumier J C et al 1993 Search for neutrinoless double-β decay in Xe with a time projection chamber Phys. Rev. D 48 100920

[15]维勒米尔 1993 用时间投影室寻找 Xe 中的无中微子双 β 衰变物理版 D 48 100920

[16] Galan J 2016 Microbulk micromegas for the search of 0νββ of Xe in the PandaX-III experiment J. Instrum.11 P04024

[16]加兰 2016 微球用于在潘达克斯三号实验装置中搜索氙的 0νββ。11 P04024

[17] Cebrián S, Dafni T, Gomez H, Herrera D C, Iguaz F J, Irastorza I G, Luzón G, Segui L and

[17]塞巴斯蒂安·斯、达芬尼·特、戈麦斯·赫、埃雷拉·德·奇、伊瓜苏·法伊、伊拉斯托扎·I G、吕宋·格、塞圭尔和

Tomás A 2013 Pattern recognition of Xe double beta decay events and background discrimination in a high pressure Xenon TPC J. Phys. G: Nucl.Part.Phys. 40 125203

2013 年氙双 β 衰变事件的模式识别和高压氙中的背景鉴别。部分。物理 40 125203

[18] Ferrario P(The NEXT collaboration) et al 2016 First proof of topological signature in the high pressure xenon gas TPC with electroluminescence amplification for the next experiment J. High Energy Phys. JHEP01(2016)104

[18]费拉里奥 P(下一个合作)等 2016 第一次证明拓扑信号在高压氙气热塑性塑料与电致发光放大为下一个实验.高能物理 JHEP01(2016)104

[19] Renner J et al 2017 Background rejection in NEXT using deep neural networks J. Instrum.12 T01004

[19]伦纳 J 等 2017 背景拒绝在下一个使用深层神经网络。12 T01004

[20] Ponkratenko O A, Tretyak V I and Zdesenko Y G 2000 The Event generator DECAY4 for simulation of double beta processes and decay of radioactive nuclei Phys. Atom.Nucl.63 12827

[20]庞克拉滕科 O A，特雷扎克第一和兹德申科 2000 事件发生器十年 4 模拟双 β 过程和放射性原子核物理原子的衰变。努克尔。63 12827

We describe in detail our particular definition of σw, although alternative definitions will certainly lead to similar results.

我们详细描述了我们对 σw 的特殊定义，尽管替代定义肯定会导致类似的结果。

34

Ponkratenko O A, Tretyak V I and Zdesenko Y G 2000 The Event generator DECAY4 for simulation of double beta processes and decay of radioactive nuclei Yad.Fiz.63 1355

2000 事件发生器，用于模拟双 β 过程和放射性原子核的衰变。Fiz。63 1355

[21] Abgrall N et al 2016 The Majorana Demonstrator radioassay program Nucl.Instrum.Methods A 828 2236

[21]阿格拉尔 N 等 2016 年马略那演示者放射性分析计划。仪器。方法 A 828 2236

[22] Ai P, Wang D, Huang G and Sun X 2018 Three-dimensional convolutional neural networks for neutrinoless double-beta decay signal/background discrimination in high-pressure gaseous time projection chamber J. Instrum.13 P08015

[22]艾平，王德，黄庚，孙 X 2018 无中微子双 β 衰变信号的三维卷积神经网络/高压气体时间投影室背景识别.13 P08015

[23] Zeng M, Li T, Cang J, Zeng Z, Fu J, Cheng J, Ma H, Liu Y and Liu Y-N 2017 3-D topological signatures and a new discrimination method for single-electron events and 0 νββ events in CdZnTe: a Monte Carlo simulation study Nucl.Instrum.Methods A 858 4452

2017 年 3-D 拓扑特征与 CdZnTe 单电子事件和 0 νββ 事件的鉴别新方法:蒙特卡罗模拟研究核。仪器。方法 A 858 4452

[24] Qiao H, Lu C Y, Chen X, Han K, Ji X D and Wang S G 2018 Signal-background discrimination with convolutional neural networks in the PandaX-III experiment using mc simulation Sci.China Phys., Mech.Astron.61 101007

[24]乔红，陆春云，陈曦，韩 k，纪晓德和王树国 2018 卷积神经网络信号背景识别在 PandaX-III 实验中的应用。中国物理机械。阿斯顿。61 101007

[25] Tomas A 2013 Development of time projection chambers with MICROMEGAS for rare event searches PhD Thesis Zaragoza U.

[25]托马斯 2013 年开发的用于罕见事件搜索的时间投影室

[26] Brun R and Rademakers F 1997 ROOT—an object oriented data analysis framework Nucl.Instrum.Methods Phys. Res. A 389 816

[26]布鲁恩和雷德梅克 1997 根——一个面向对象的数据分析框架。仪器。方法物理学报 A 389 816

[27] Agostinelli S et al 2003 GEANT4: a simulation toolkit Nucl.Instrum.Methods A 506 250303

[27]阿戈斯蒂内利 S 等 2003 GEANT4:一个模拟工具包 Nucl。仪器。方法 A 506 250303

[28] Pfeiffer D et al 2019 Interfacing Geant4, Garfield++ and Degrad for the simulation of gaseous detectors Nucl.Instrum.Meth.A 935 12134

[28]普发等人 2019 年接口 Geant4，加菲尔德++和 Degrad 模拟气体探测器 Nucl。仪器。冰毒。A 935 12134

[29] Galan J 2016 REST v2.0: a data analysis and simulation framework for micro-patterned readout detectors 8th Sym.on Large TPCs for Low-Energy Rare Event Detection

[29]加兰 J 2016 REST v2.0:微模式读出检测器的数据分析和模拟框架第 8 代 Sym。用于低能稀有事件探测的大型光子晶体

[30] Held M and Karp R M 1962 A dynamic programming approach to sequencing problems J. Soc.Ind.Appl. Math.10 196210

[30]霍尔德 1962 一种解决排序问题的动态规划方法。印度。应用数学。10 196210

[31] Applegate D L, Bixby R E, Chvatal V and Cook W J 2007 The Traveling Salesman Problem: A Computational Study (Princeton Series in Applied Mathematics) (Princeton, NJ: Princeton University Press)

[31]阿普尔盖特 D L，比克斯比 R E，奇瓦塔尔 V 和库克 W J 2007 旅行推销员问题:计算研究(普林斯顿应用数学系列)(普林斯顿，新泽西州:普林斯顿大学出版社)

[32] Chytracek R, McCormick J, Pokorski W and Santin G 2006 Geometry description markup language for physics simulation and analysis applications IEEE Trans.Nucl.Sci.53 2892

2006 物理模拟和分析应用的几何描述标记语言。努克尔。Sci。53 2892

[33] Biagi S F 1999 Nucl.Instrum.Meth.A 421 23440

[33]比亚吉 1999 年成立。仪器。冰毒。A 421 23440

[34] Borges F I G M and Conde C A N 1996 Experimental W-values in gaseous Xe, Kr and Ar for low energy x-rays Nucl.Instrum.Methods Phys. Res. A 381 916

[34]博尔热斯·I G·M 和康德·C·A·N 1996 低能 x 射线核在气态氙、氪和氩中的实验钨值。仪器。方法物理学报 A 381 916

35